Supporting Information for

Synthetic Models for the [FeFe]-Hydrogenase: Catalytic Proton Reduction and the Structure of the Doubly Protonated Intermediate

Maria E. Carroll, Bryan E. Barton, Thomas B. Rauchfuss*, Patrick J. Carroll

Contents

p4. Spectroscopic Data

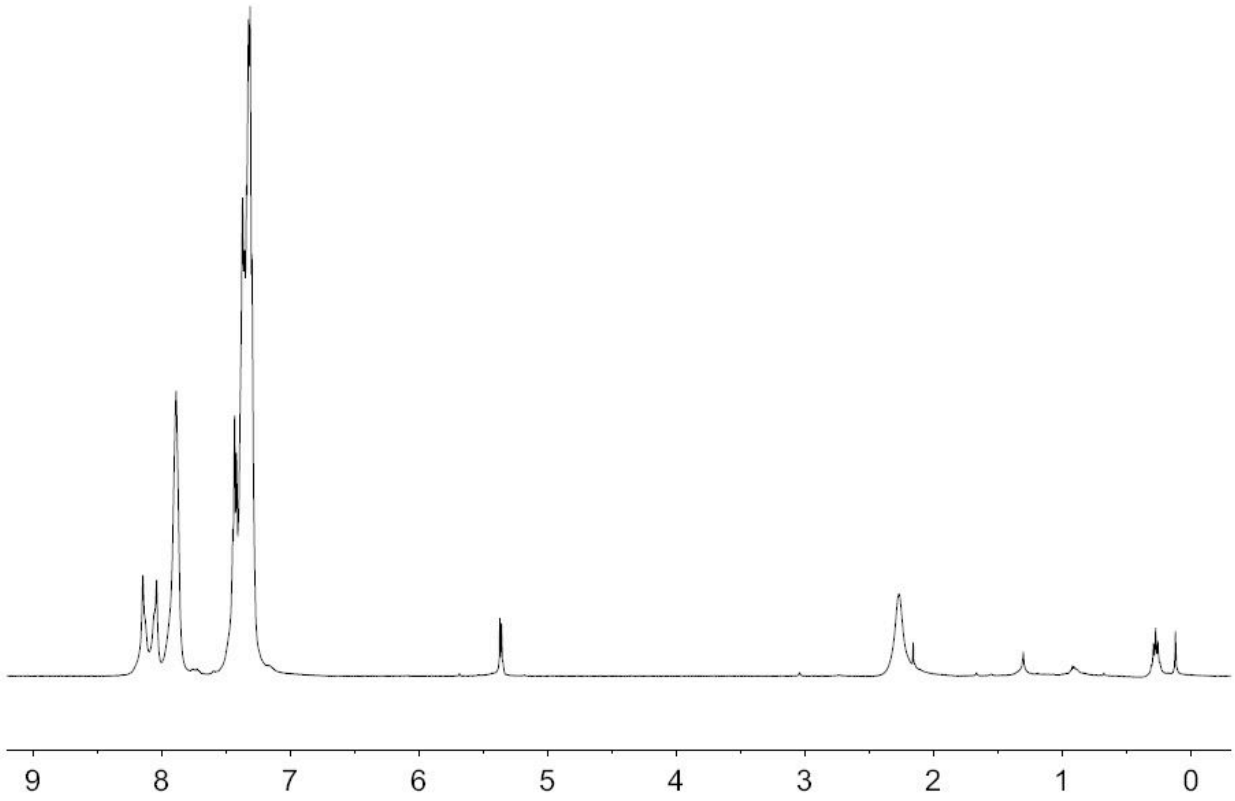

Figure S1. ^{1}H NMR spectrum of $Fe_2(adt^{NH})(CO)_2(dppv)_2$, **1**$^{\mathbf{NH}}$.

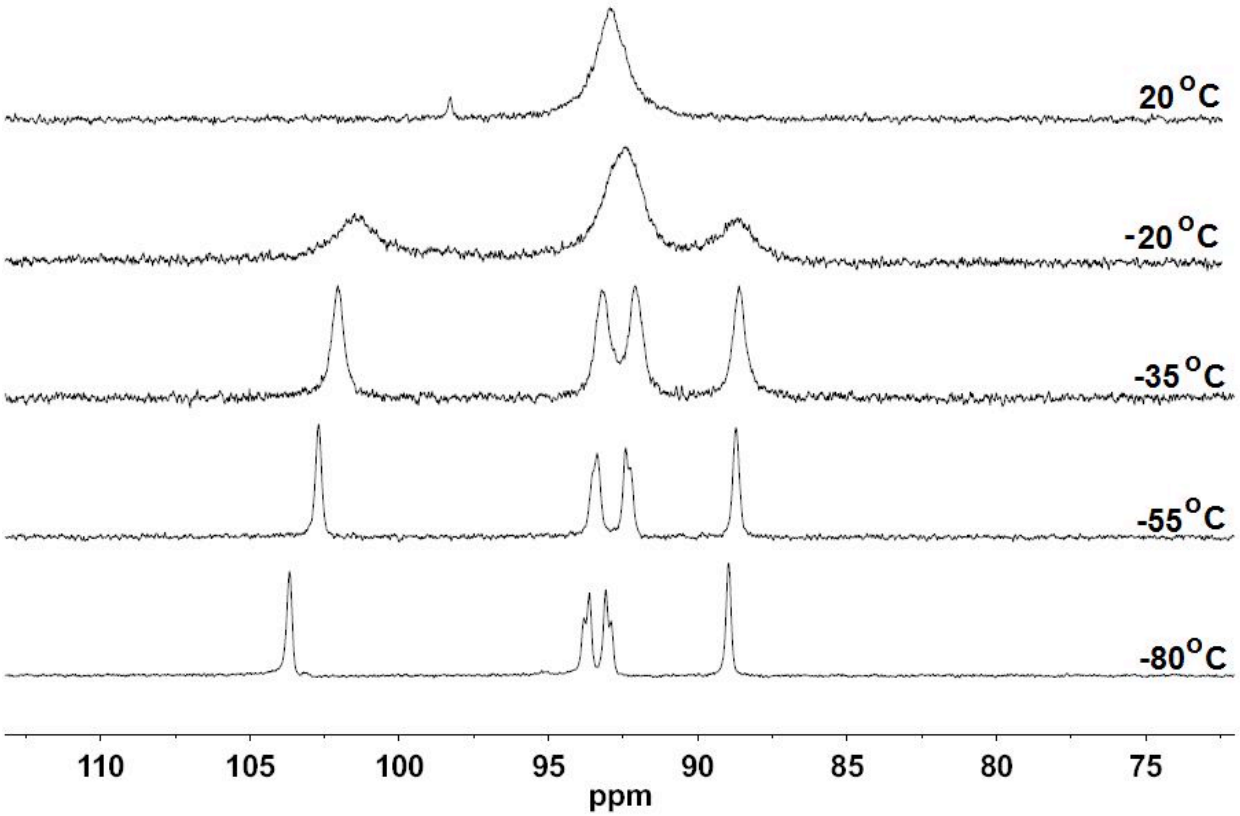

Figure S2. Variable temperature ^{31}P NMR spectrum of $\mathbf{1}^{NH}$ in CD_2Cl_2.

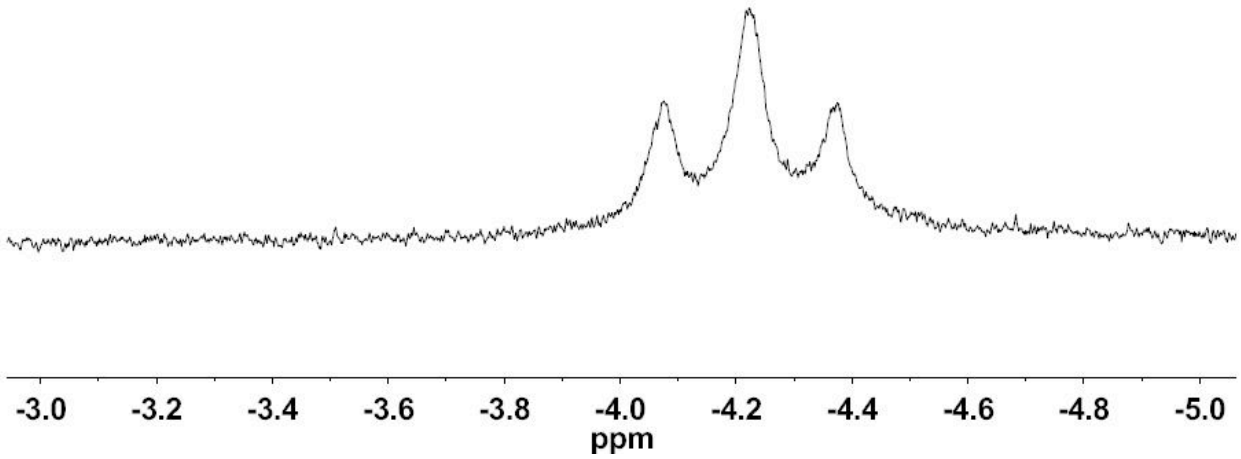

Figure S3. High field ^{1}H NMR spectrum of [*t*-H**1**$^{\mathbf{NH}}$]BAr$^{F}_{24}$ in CD_2Cl_2 at -80 °C.

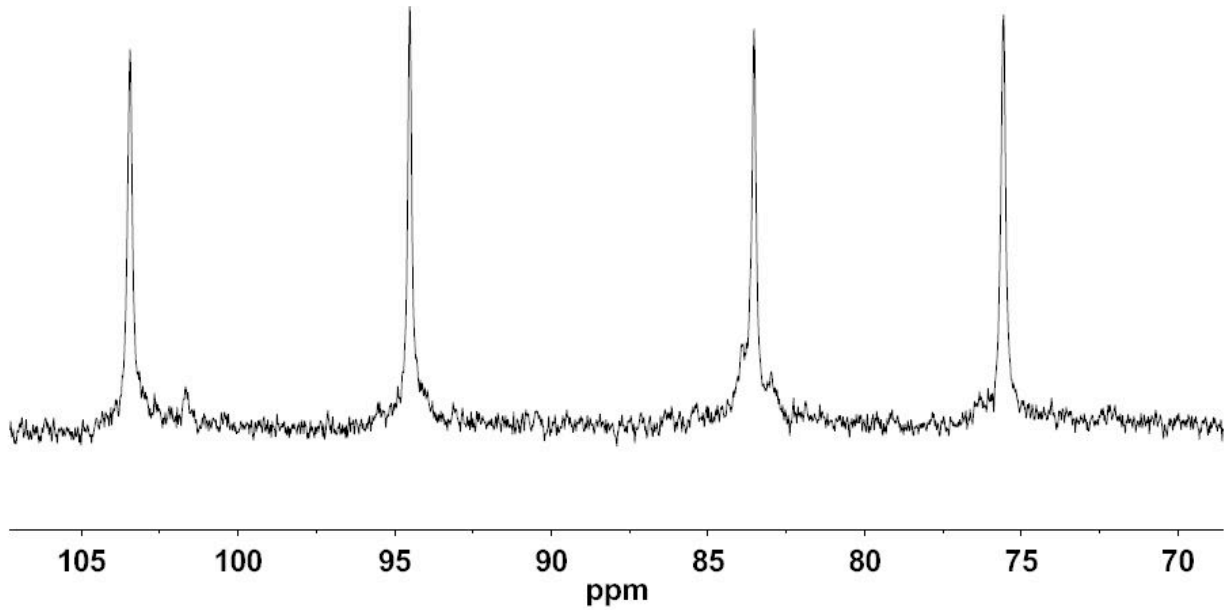

Figure S4. ^{31}P NMR spectrum of [*t*-H**1**$^{\mathbf{NH}}$]BAr$^{F}_{24}$ in CD_2Cl_2 at -80 °C.

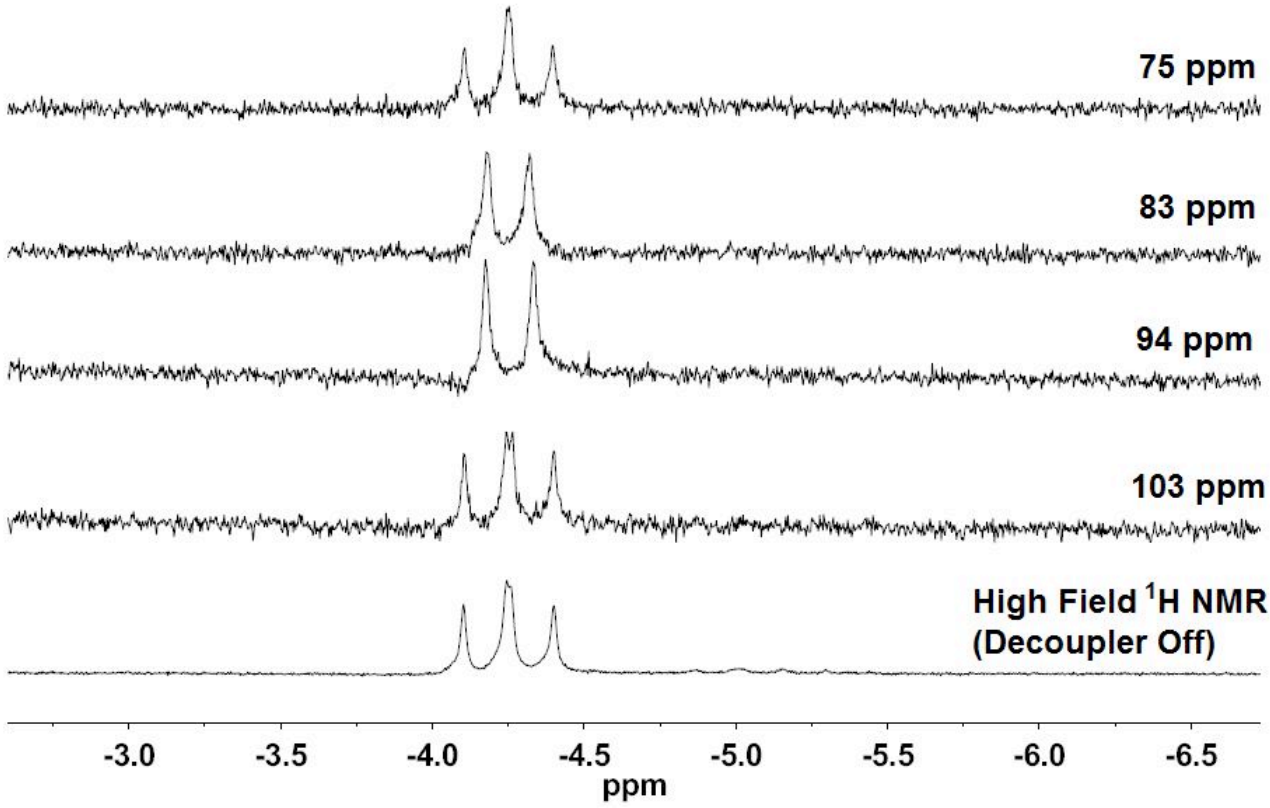

Figure S5. High field region of ^{31}P Decoupled ^{1}H NMR of [*t*-H**1**$^{\mathbf{NH}}$]BAr$^{F}_{24}$ (Chemical shift listed corresponds to the ^{31}P NMR signal to which the spectrum is decoupled)

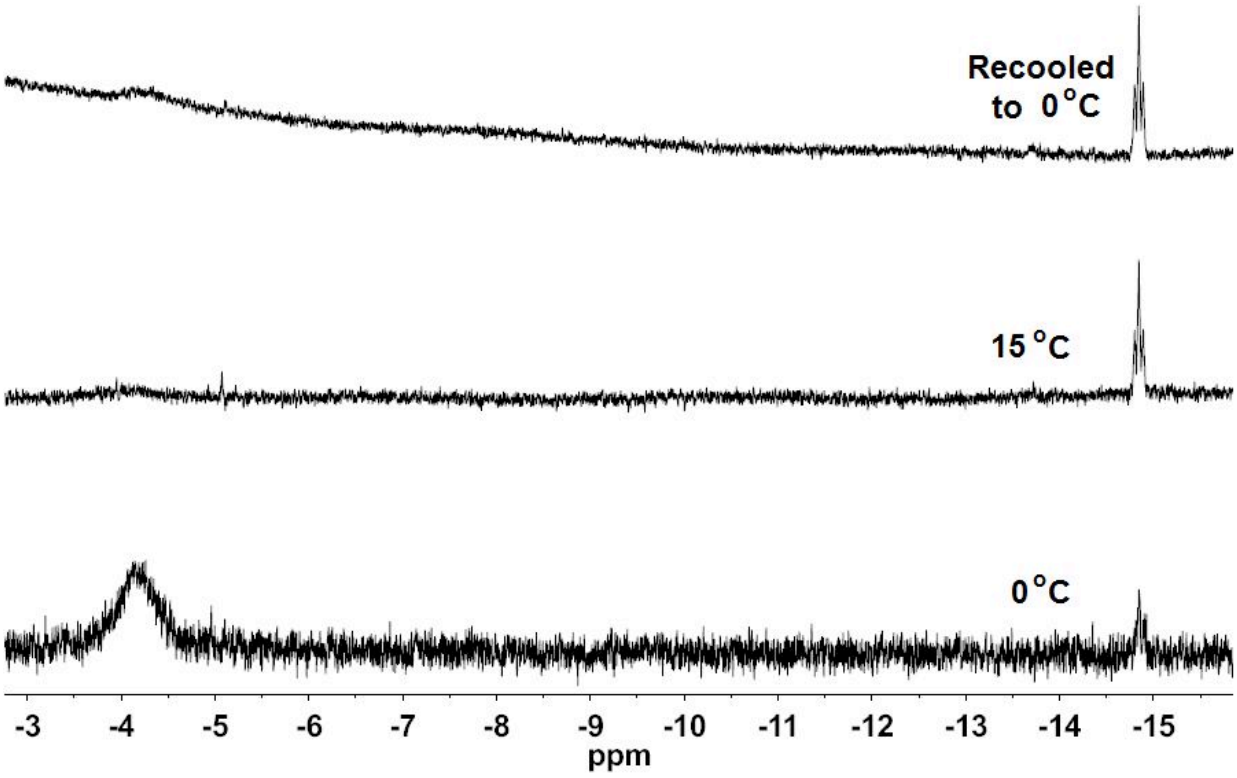

Figure S6. High field region ^{1}H NMR spectra of [*t*-H**1**^{NH}]BAr$^{F}_{24}$ and sym-[μ-H**1**^{NH}]BAr$^{F}_{24}$. At 0 °C [*t*-H**1**^{NH}]BAr$^{F}_{24}$ is the major species. Upon warming to 15 °C, sym-[μ-H**1**^{NH}]BAr$^{F}_{24}$ is the major species. Upon recooling to 0 °C, sym-[μ-H**1**^{NH}] BAr$^{F}_{24}$ is still the major species, showing that once isomerization to the bridging hydride occurs, the terminal hydride cannot be reformed.

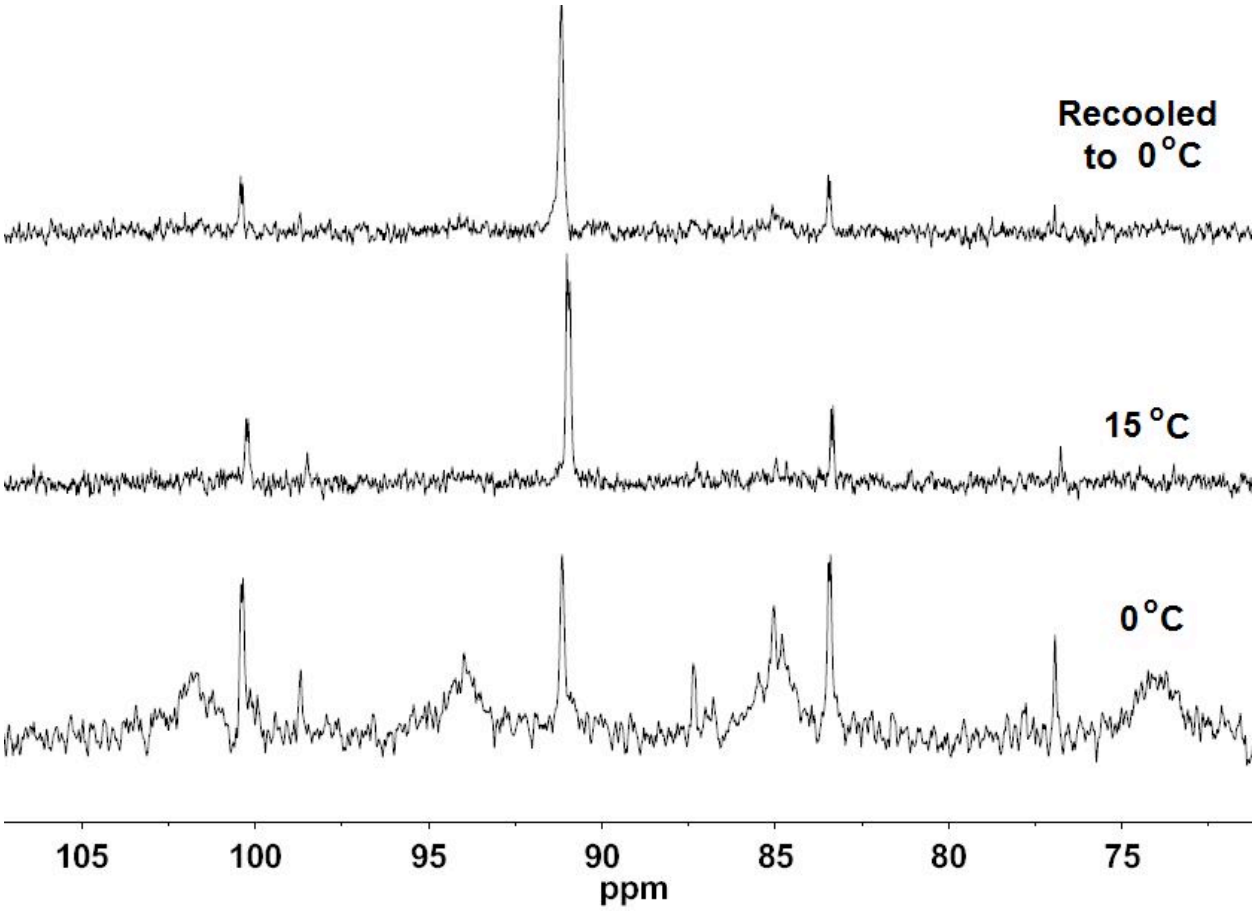

Figure S7. ^{31}P NMR spectra of [*t*-H**1**^{NH}]BAr$^{F}_{24}$ and *sym*-[μ-H**1**^{NH}]BAr$^{F}_{24}$. At 0 °C [*t*-H**1**^{NH}]BAr$^{F}_{24}$ is the major species. Upon warming to 15 °C, *sym*-[μ-H**1**^{NH}]BAr$^{F}_{24}$ is the major species. Upon recooling to 0 °C, *sym*-[μ-H**1**^{NH}]BAr$^{F}_{24}$ is still the major species, showing that once isomerization to the bridging hydride occurs, the terminal hydride cannot be reformed.

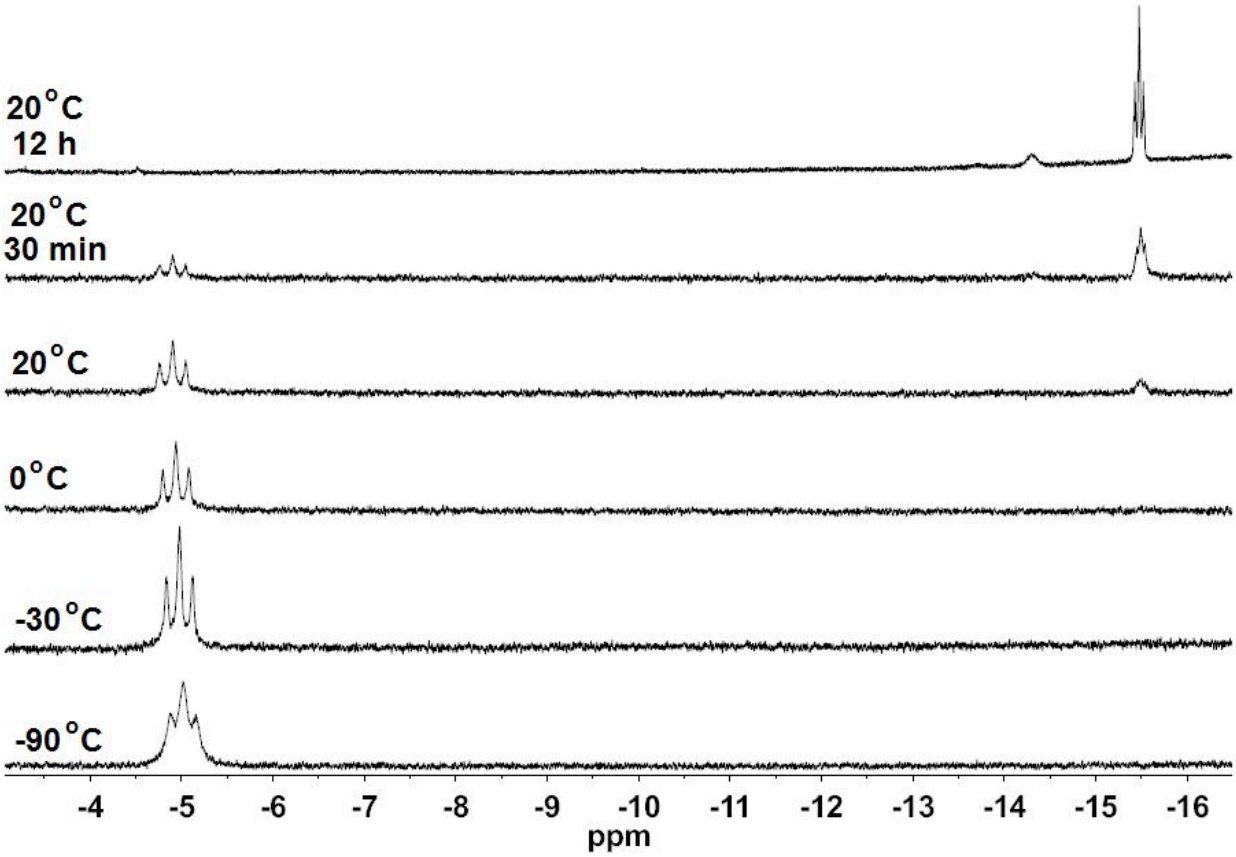

Figure S8. Variable temperature high field ^{1}H NMR spectrum of **1**^{NH} + 2 equiv $[H(Et_2O)_2]BAr^F{}_{24}$ in CD_2Cl_2.

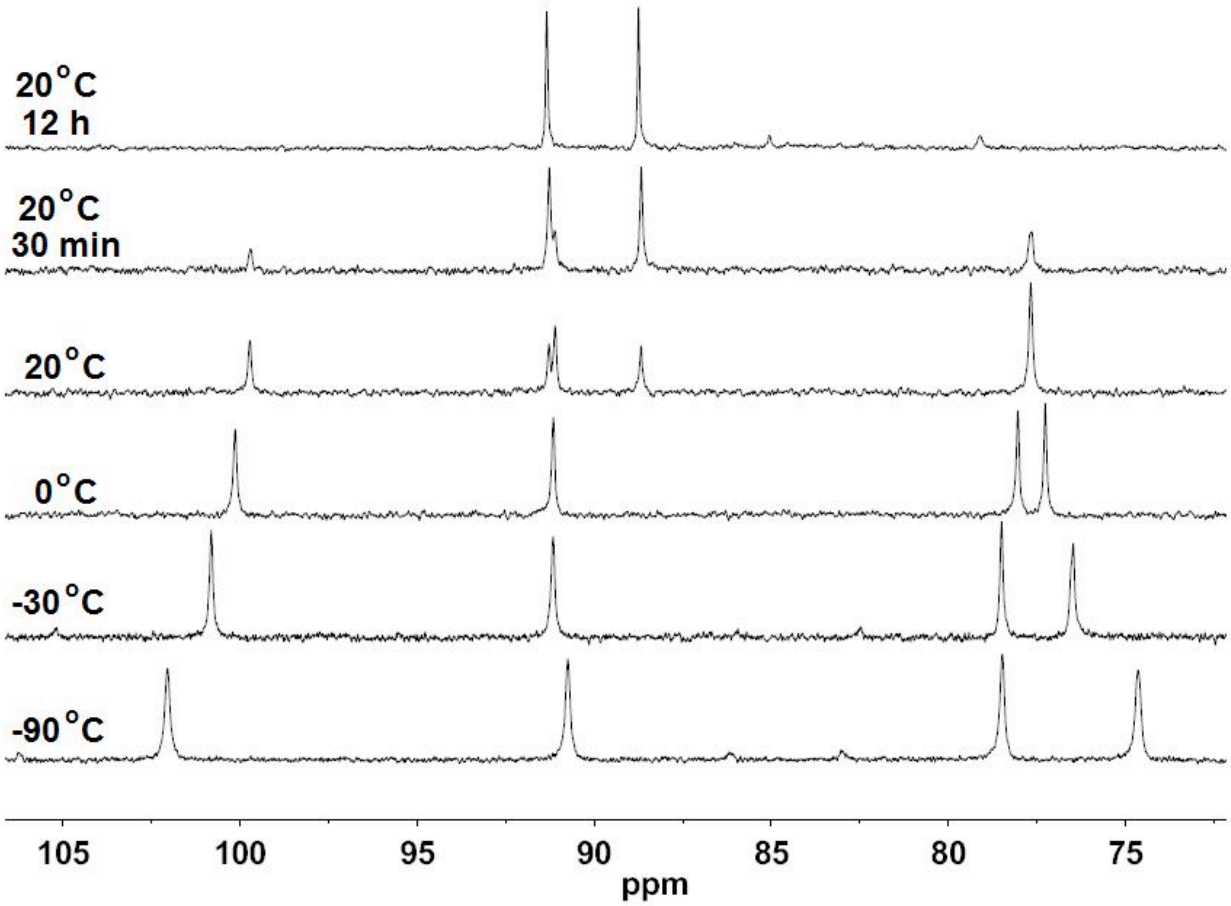

Figure S9. Variable temperature ^{31}P NMR spectrum of **1**^{NH} + 2 equiv $[H(Et_2O)_2]BAr^F{}_{24}$ in CD_2Cl_2.

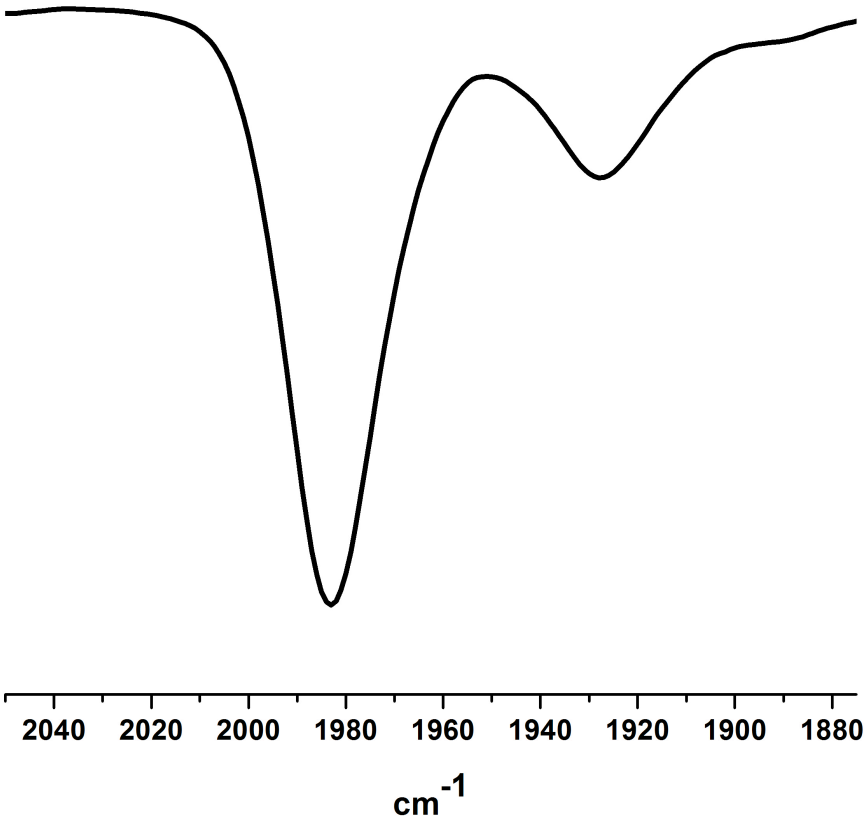

Figure S10. IR spectrum of [*t*-H**1**^{NH2}]$^{2+}$ formed by protonation of **1**^{NH} with 2 equivalents of $HBF_4 \cdot Et_2O$ in CH_2Cl_2 at 0 °C.

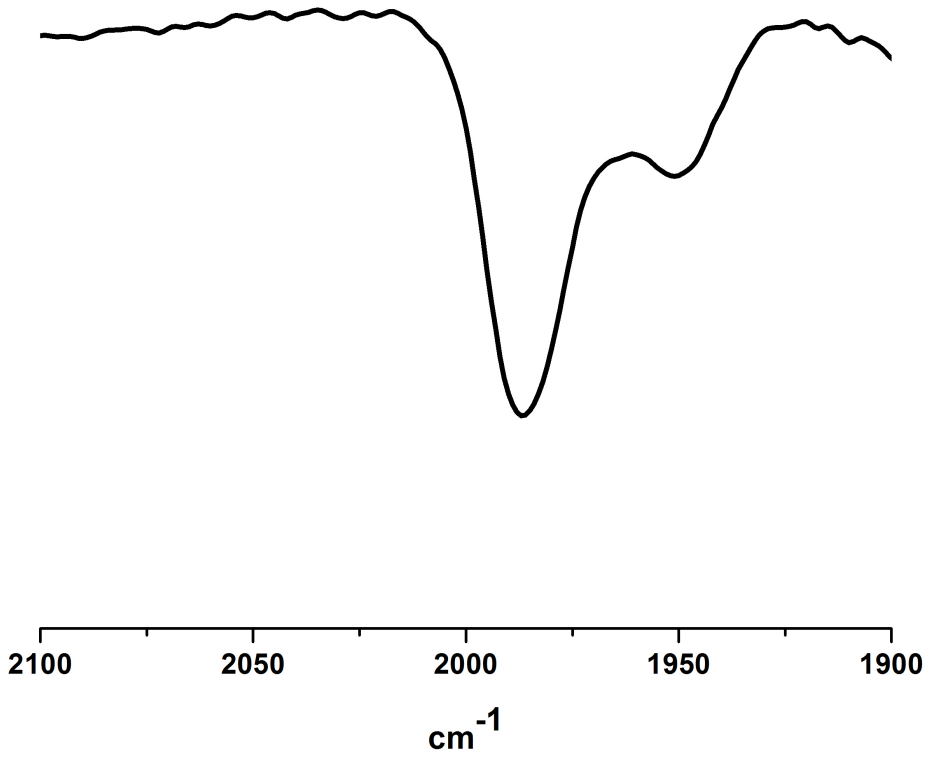

Figure S11. IR spectrum of [*t*-H**1**H]$^{2+}$ formed by protonation of **1**^{NH} with 2 equiv of CF_3COOH in CH_2Cl_2 at -78 °C.

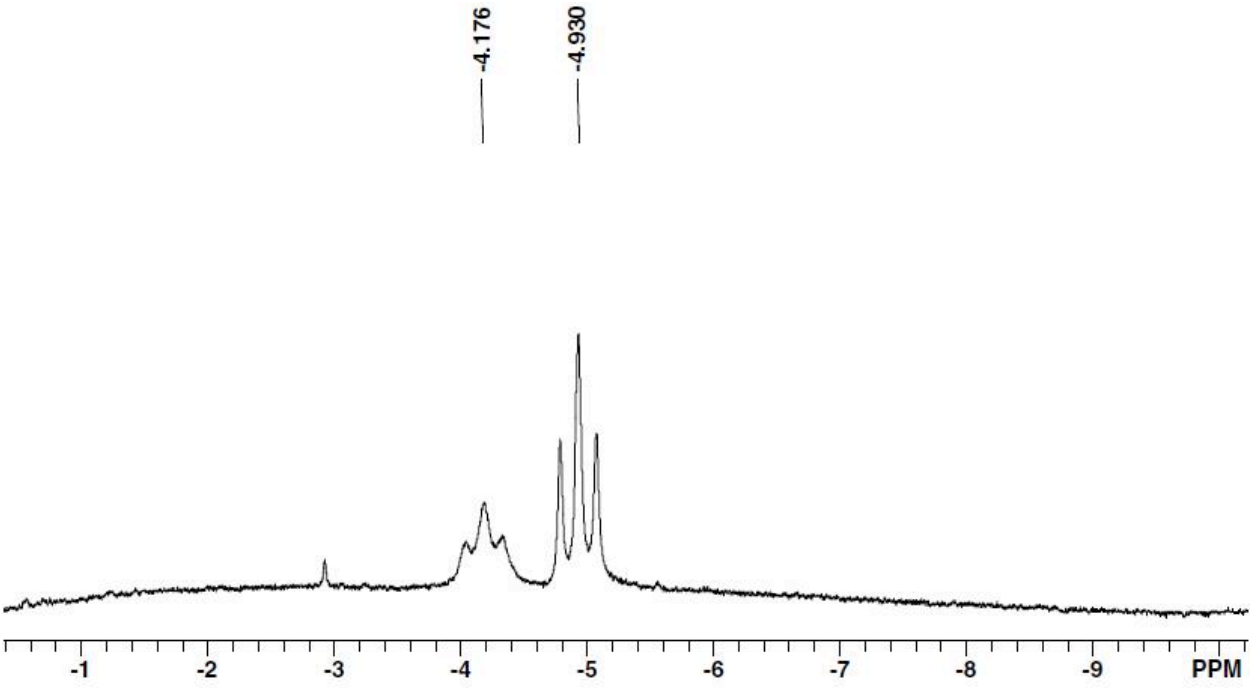

Figure S12. High field ^{1}H NMR spectra of a mixture of [*t*-H**1**$^{\mathbf{NH}}$]BAr$^{F}_{24}$ and [*t*-H**1**$^{\mathbf{NH2}}$](BAr$^{F}_{24}$)$_2$ in CD_2Cl_2 at -40 ºC.

a.

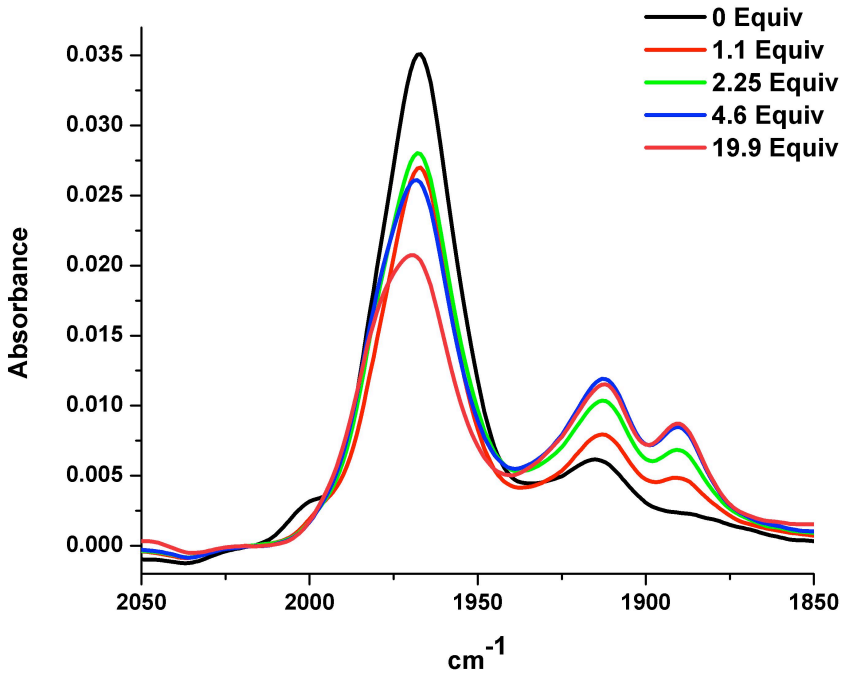

b.

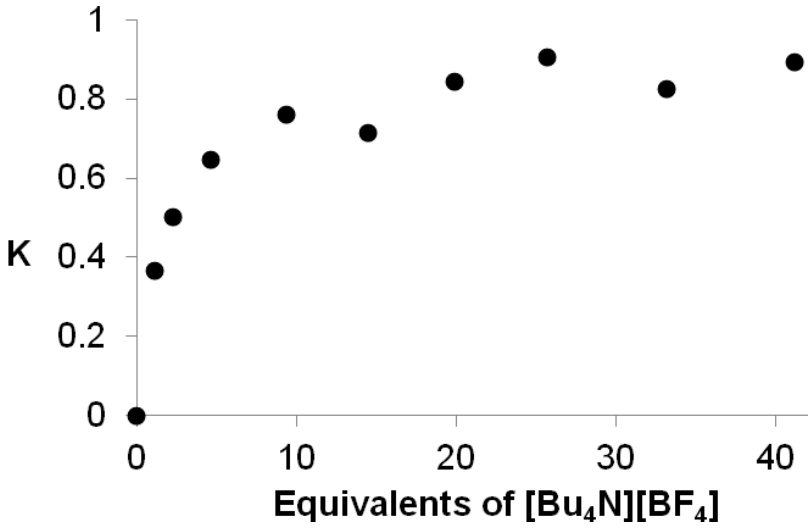

Figure S13. a. IR spectra of a solution of [*t*-H**1**^{NH}]BAr$^{F}_{24}$ with 0, 1, 2, 3, 10 equiv of added [Bu$_4$N]BF$_4$ at -78 °C b. Graph of K (the equilibrium ratio of [*t*-H**1**^{NH}]$^+$/[H**1**^{NH}]$^+$) vs. equivalents BF_4^- for a CH_2Cl_2 solution of [*t*-H**1**^{NH}]BAr$^{F}_{24}$.

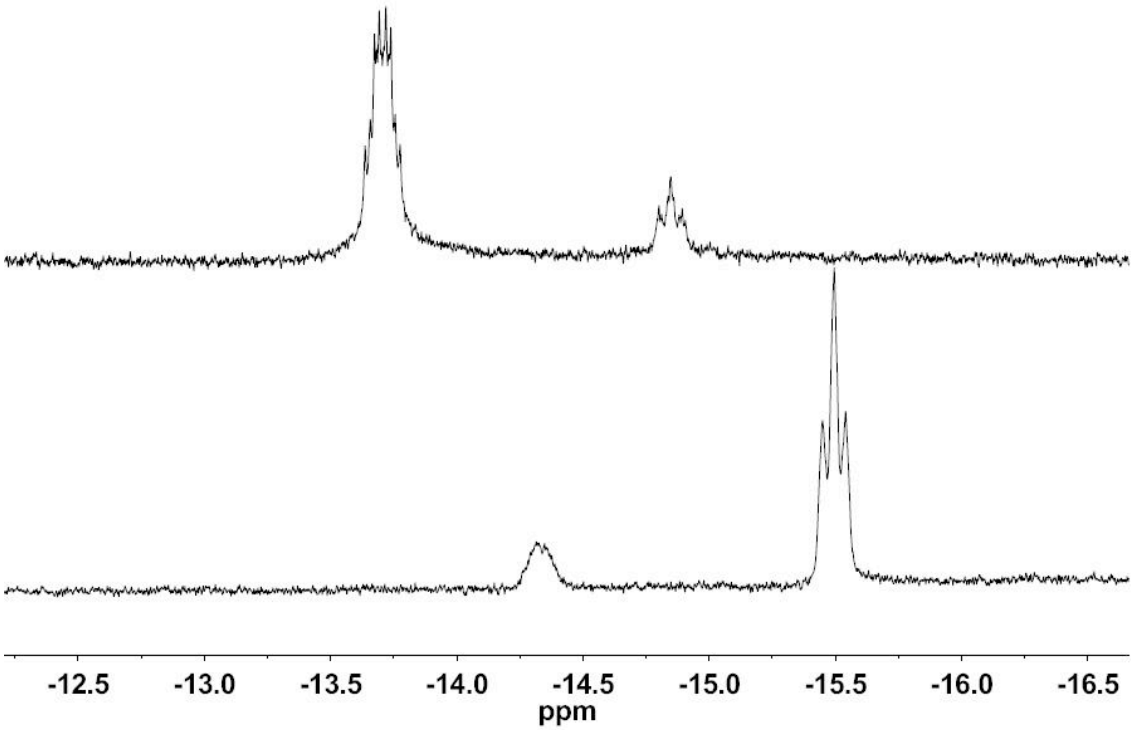

Figure S14. High field ^{1}H NMR spectra of [μ-H**1**$^{\mathbf{NH}}$]$^{+}$ (top) and [μ-H**1**$^{\mathbf{NH2}}$]$^{2+}$ (bottom) in CD_2Cl_2.

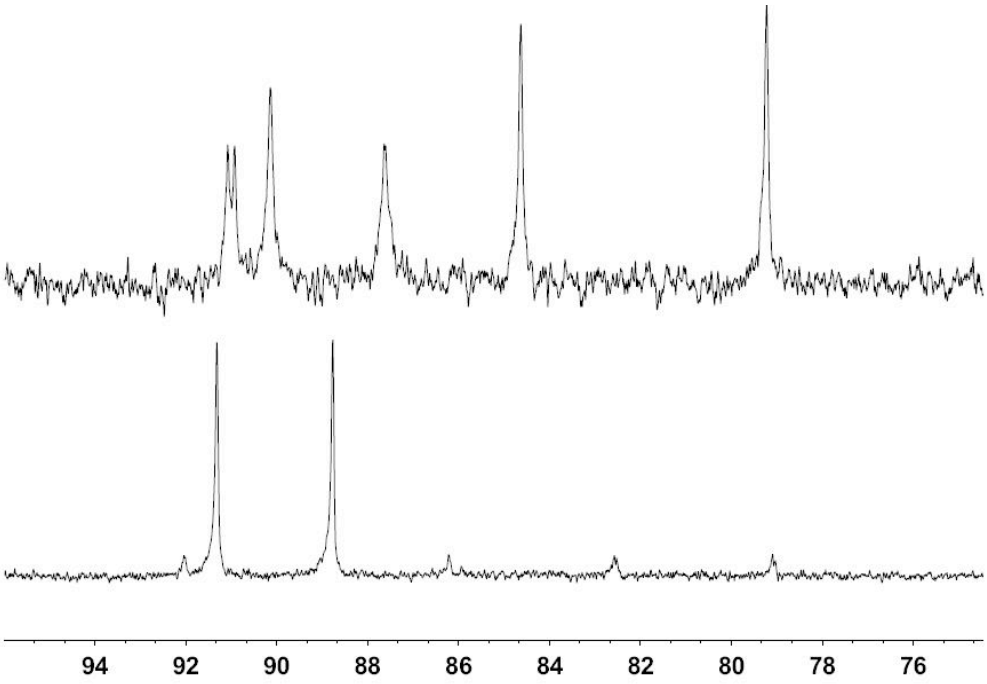

Figure S15. ^{31}P NMR spectra of [μ-H**1**$^{\mathbf{NH}}$]$^{+}$ (top) and [μ-H**1**$^{\mathbf{NH2}}$]$^{2+}$ (bottom) in CD_2Cl_2.

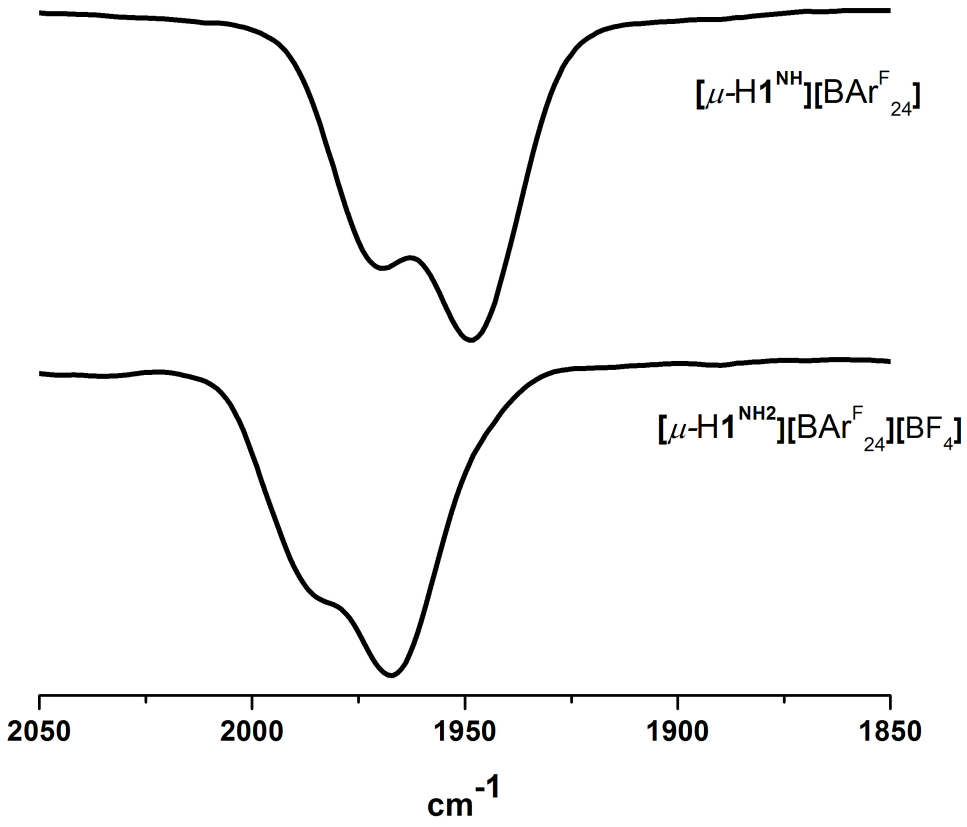

Figure S16. IR spectra of $[Fe_2(adt^{NH})(\mu\text{-H})(CO)_2(dppv)_2]^+$ ($[\mu\text{-H}\mathbf{1}^{\mathbf{NH}}]^+$) and $[Fe_2(adt^{NH2})(\mu\text{-H})(CO)_2(dppv)_2]^{2+}$ ($[\mu\text{-H}\mathbf{1}^{\mathbf{NH2}}]^{2+}$) in CH_2Cl_2

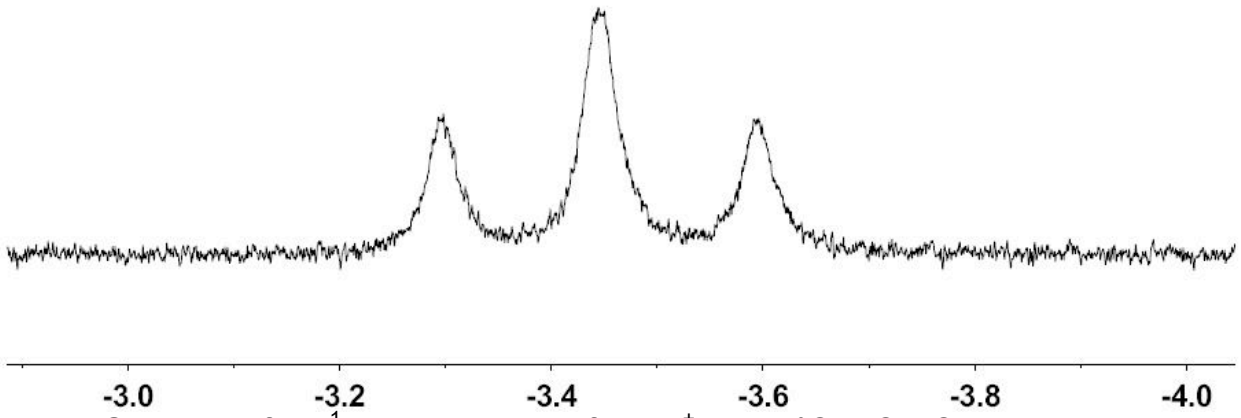

Figure S17. High field ^{1}H NMR spectra of [*t*-H**2**]$^{+}$ at -90 °C in CD_2Cl_2.

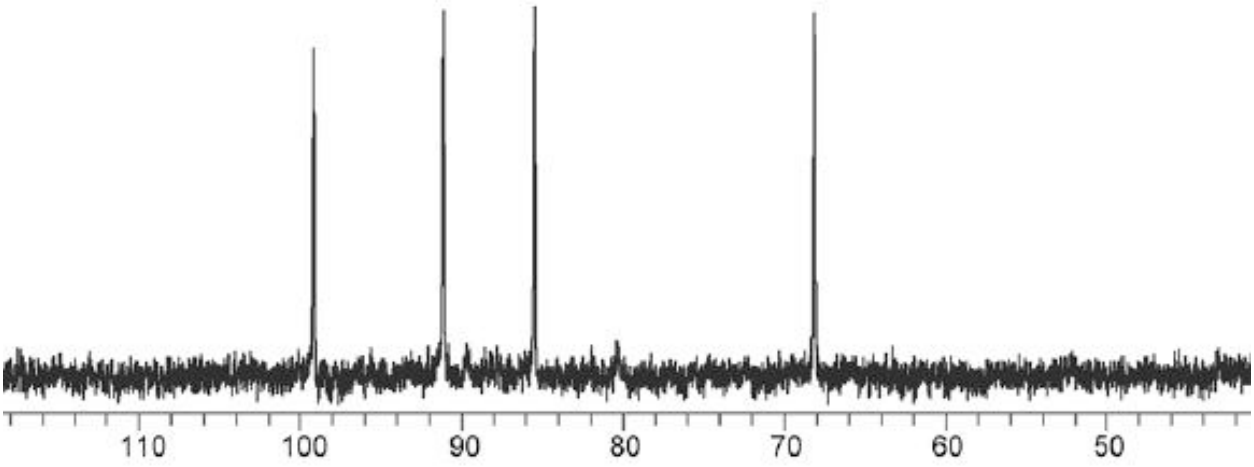

Figure S18. ^{31}P NMR spectra of [*t*-H**2**]$^{+}$ at -90 °C in CD_2Cl_2.

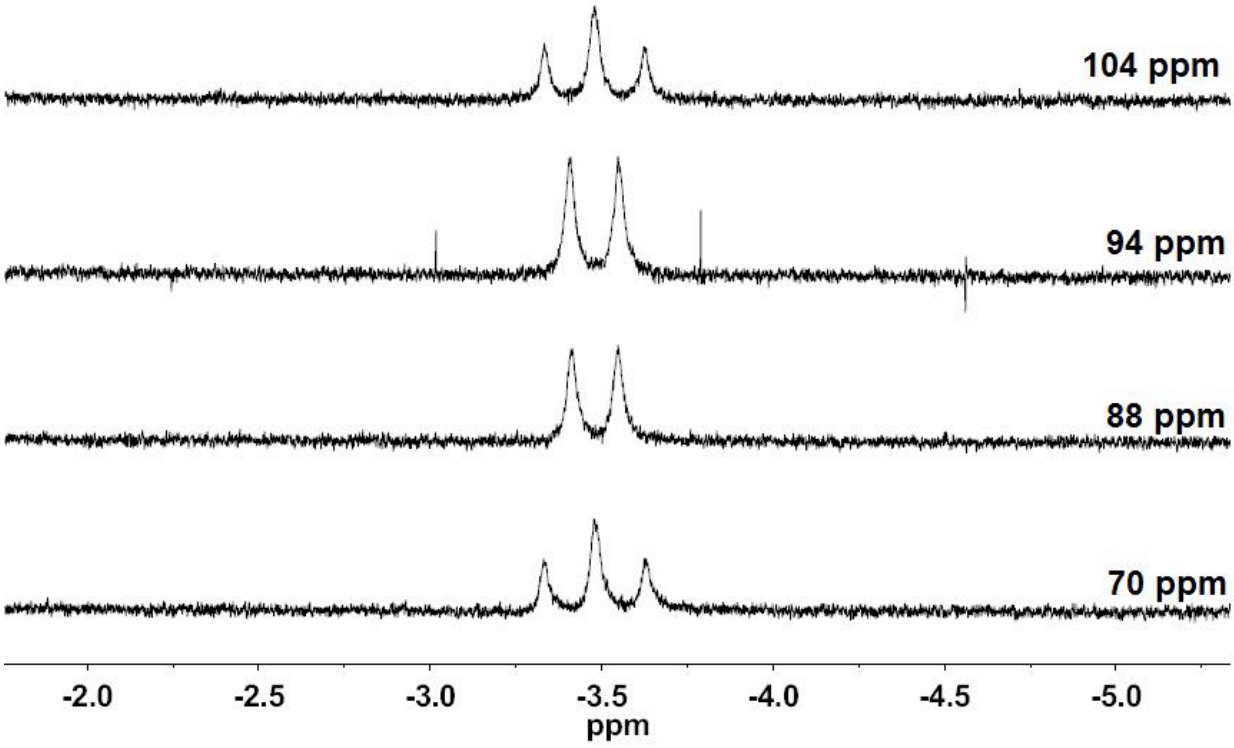

Figure S19. High field region of ^{31}P Decoupled ^{1}H NMR of [*t*-H**2**]BAr^{F}_{24} at -90 °C (Chemical shift listed corresponds to the ^{31}P NMR signal to which the spectrum is decoupled)

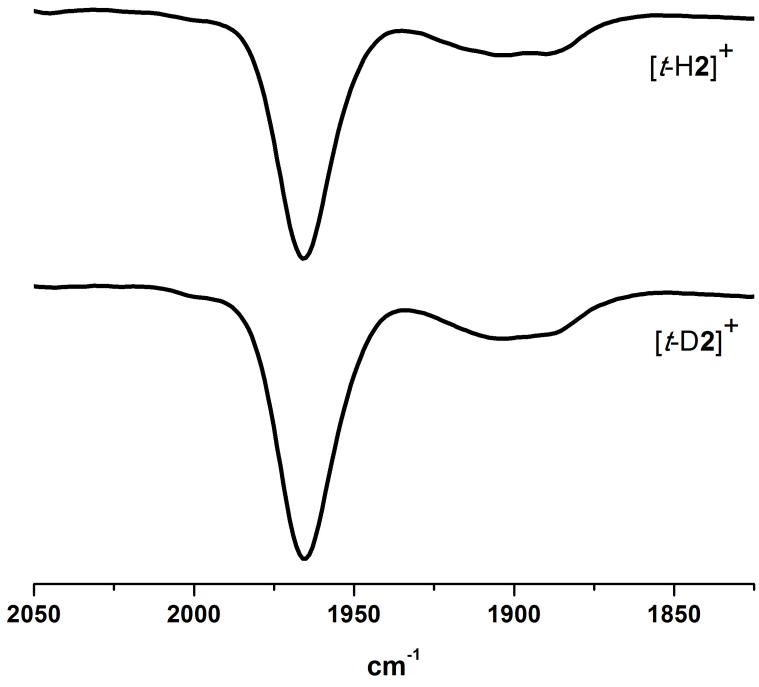

Figure S20. IR spectra of [*t*-H**2**]$^+$ and [*t*-D**2**]$^+$ formed by protonation of **2** with excess $[H(Et_2O)_2]BAr^F{}_{24}$ and $[D(Et_2O)_2]BAr^F{}_{24}$, respectively, in CH_2Cl_2 at -78 $^\circ$C.

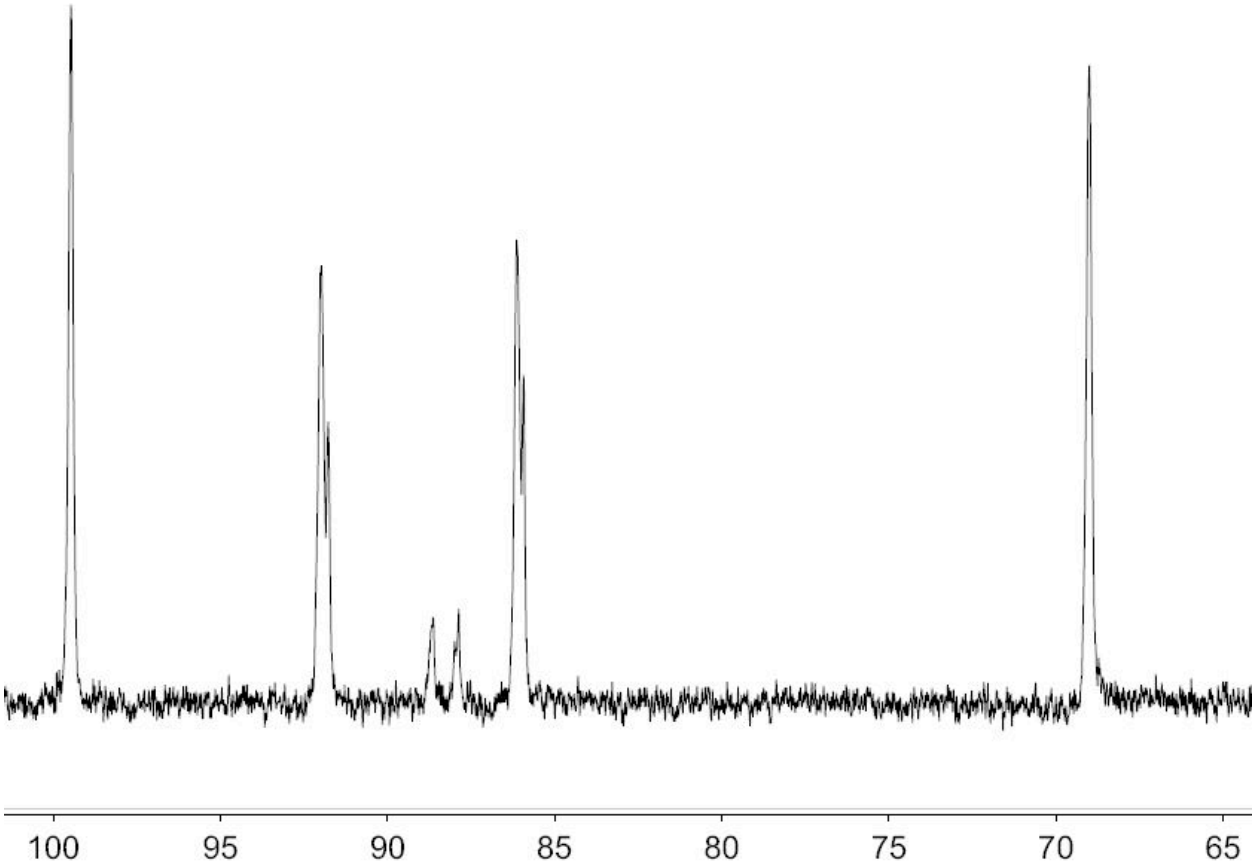

Figure S21. ^{31}P NMR spectrum [*t*-D**2**]$^{+}$ at -20 °C, formed by protonation of **2** with excess $[D(Et_2O)_2]BAr^F{}_{24}$ in CH_2Cl_2. Splitting of the signals at 86 and 91 ppm is due to coupling of these phosphorus centers with the terminal deuteride. Signals at 88 and 89 ppm are due to the bridging deuteride, [μ-D**2**]$^{+}$.

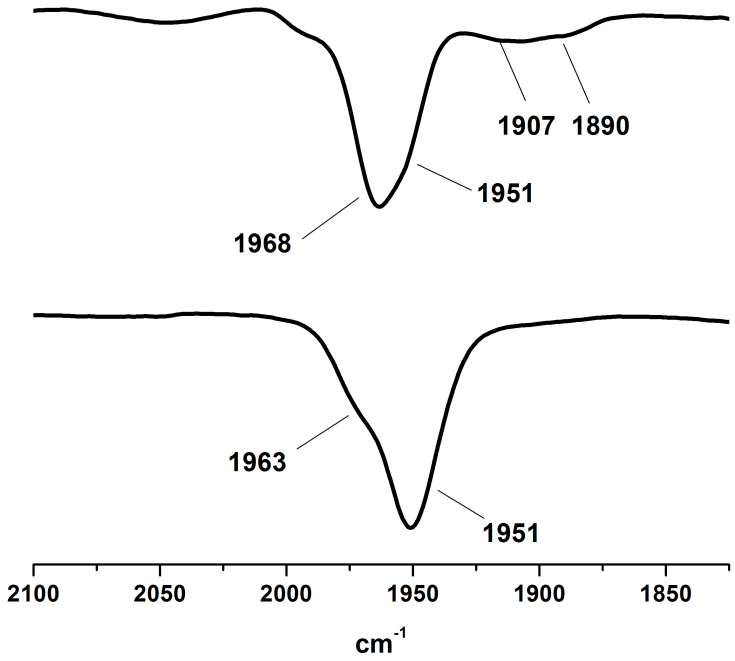

Figure S22. Top: IR spectrum of a mixture of [*t*-H**2**]$^+$ (ν_{co}= 1968, 1907, 1890 cm^{-1}) and [μ-H**2**]$^+$ (ν_{co}= 1951 cm^{-1}) formed by protonation of **2** with excess $HBF_4 \cdot Et_2O$ at room temperature in CH_2Cl_2. IR spectrum was acquired immediately after addition of acid. Bottom: IR spectrum of mixture after stirring at room temperature overnight, showing that [μ-H**2**]$^+$ is the only species present.

The IR spectrum of [*t*-H**2**]$^+$ exhibits a strong band at 1965 cm^{-1} (terminal CO), 1905 cm^{-1} (bridging CO), and 1890 cm^{-1}, which we initially assigned as an Fe-H stretch. However, the deuteride, [*t*-D**2**]$^+$ has the same IR spectrum (See Figure S20). The ^{31}P NMR spectrum of [*t*-D**2**]$^+$ is identical to that for [*t*-H**2**]$^+$, except that P-D coupling is apparent. (See Figure S21). The IR spectrum of [μ-H**2**]$^+$ only contains ν_{co}= 1951, 1963 cm^{-1}, indicating that the bands at 1890 and 1905 cm^{-1} in the spectrum of [*t*-H**2**]$^+$ are attributed to the terminal hydride species. We propose that the weak bands at 1905 and 1890 cm^{-1} are due to the presence of two flippamers and are both due to semi-bridging CO ligands, as shown below.

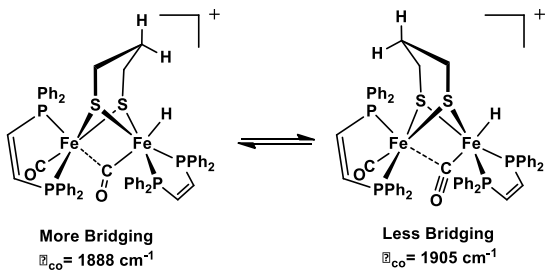

Experimental Details.

Determination of pK_a of $[HFe_2(adt)(CO)_2(dppv_2)]^+$.

As discussed in the paper, we estimate the pK_a of [*t*-H**1**^{NH}]$^+$ to be between 15.3 and 17.6, on the MeCN pK_a scale. A pK_a scale in CD_2Cl_2 has been established for a number of phosphonium tetrafluoroborate salts.[1] At -90 °C, **1**^{NH} is protonated by $[HPMe_2Ph]BF_4$ (pK_a^{CD2Cl2} = 5.7) to form [*t*-H**1**^{NH}]$^+$, but **1** is not protonated by $[HPBu_3]BF_4$ (pK_a^{CD2Cl2} = 8.4). Therefore, on the scale in CD_2Cl_2 we can bracket the pK_a of [*t*-H**1**^{NH}]$^+$ between 5.7 and 8.4.

General Procedures for Proton Reduction Catalysis.

Voltammograms were recorded at varying [H$^+$]/catalyst ratios. Plots of i_c/i_p vs equiv of acid, where i_c is the peak current of the reduction wave in the presence of acid (Eq 1) and i_p is the peak current in the absence of acid (Eq 2), are initially linear, indicating a second order dependence on acid (i.e. hydrogen evolution occurs via protonation of a metal hydride). At some value of [H$^+$], these plots reach a "plateau region", in which the value of i_c, and therefore i_c/i_p, no longer increases with increasing amounts of acid. The rate constant deduced for this acid-independent plateau can be evaluated from Eq 3.[2,3] As defined in eq 2, the value of i_c is independent of scan rate. Studies on the scan rate dependence of i_c show that scan rate independence is only achieved at scans rates of 0.5 V/s and greater (See Figures S32, 33, 38).

$$i_c = nFA[\text{cat}]\sqrt{D(k[\text{H}^+])} \quad \text{Equation 1}$$

$$i_p = 0.4463FA[\text{cat}]\sqrt{\frac{F\upsilon D}{RT}} \quad \text{Equation 2}$$

$$\frac{i_c}{i_p} = \frac{n}{0.4463}\sqrt{\frac{RTk}{F\upsilon}} \quad \text{Equation 3}$$

where n = # electrons

υ = scan rate in V/s

F = Faraday's constant (96485 C/s)

R = gas constant (8.314 J/mol•K)

T = temperature in K

k = first order rate constant for H_2 evolution in $[H^+]$-independent region.

i_c = max. current in presence of acid

i_p = max. current in absence of acid

For this work, overpotential is defined as the difference between the reduction potential of the acid ($E°_{HA/H2}$) and the potential at which the catalyst reduces the same acid (E_{cat}).[4,5] For each acid concentration, E_{cat}, the maximum of the first derivative of the forward scan minus 15 mV, was determined in the region in which i_c is linearly dependent on the concentration of acid. The $E°_{cat}$ value used in overpotential calculations is the average of the values at each acid concentration. The values of $E°_{HA/H2}$ were calculated based on the method from Fourmond et al, with corrections for homoconjugation.[5] When determining the overpotential for [*t*-H**2**]$^+$, $E°_{HA/H2}$ for HBF_4•Et_2O was calculated using a pK_a value of 2.1, that for perchloric acid.[5] We assume similar dissociation of the two acids.

Determining the overpotential for the systems discussed here is complicated by the fact that catalysis is performed in CH_2Cl_2 in which the standard reduction potentials of the acids are unknown. Therefore, the overpotentials for catalysis by these diirion hydrides are estimates. Under conditions used for catalysis by [*t*-H**1**^{NH}]$^+$, we found that a Pt electrode catalyzed the reduction of chloroacetic acid at -1.0 V vs $Fc^{+/0}$, in good agreement with -1.05 V reported for the reduction of this acid in MeCN solution.[4]

Scan Rate Dependence for catalysis by [*t*-HFe$_2$(adt^{NH})(CO)$_2$(dppv$_2$)]$^+$, [*t*-H1^{NH}]$^+$. A 2-mL CH_2Cl_2 solution of 1.0 mM **1** (2.1 mg, 0.002 mmol), 0.125 M $[Bu_4N]PF_6$, and a ferrocene reference was cooled to 0 °C and treated with 600 μL of 2.0 M H_2ClCCO_2H (600 equiv). Cyclic voltammograms were obtained at a range of scan rates (See Figures S32, 33).

Catalyst Concentration Dependence for [*t*-HFe$_2$(adt^{NH})(CO)$_2$(dppv$_2$)]$^+$, [*t*-H1^{NH}]$^+$. A 1.5-mL CH_2Cl_2 solution of 1.0 mM **1**^{NH} (1.5 mg, 0.0015 mmol), 0.125 M

$[Bu_4N]PF_6$, 0.67 M $H_2ClC_2O_2H$ (667 equiv), and a ferrocene reference was cooled to 0 °C. A cyclic voltammogram was obtained at ν = 1 V/s. To the solution, 0.5 mL aliquots of a 0.125 M $[Bu_4N]PF_6$ were added, and a CV was collected at each concentration(See Figure S34).

Proton Reduction Catalysis by $[t\text{-}HFe_2(adt^{NH})(CO)_2(dppv_2)]^+$, $[t\text{-}H1^{NH}]^+$. A 2-mL CH_2Cl_2 solution of $\mathbf{1}^{NH}$ (2.0 mg, 0.002 mmol) and $[NBu_4]BAr^F{}_{24}$ (276 mg, 0.25 mmol) was cooled to 0 ºC. A CV was recorded in the absence of acid, in order to obtain a value for i_p. The solution was then treated with aliquots of a 2 M solution of HCl_2CCO_2H in CH_2Cl_2 via a micropipette. After each addition, a CV was collected at ν= 0.5 V/s, and the value of i_c was recorded. Addition of acid continued until the value of i_c/i_p remained constant. A similar experiment was performed in MeCN solution, in which case, a second reduction wave is observed at -1.8 V that also increases with addition of acid. The species responsible for this wave is unknown (See Figure S36).

Proton Reduction Catalysis by $[t\text{-}DFe_2(adt^{NH})(CO)_2(dppv)_2]^+$, $[t\text{-}D1^{NH}]^+$. A 2-mL CH_2Cl_2 solution of $\mathbf{1}^{NH}$ (2.0 mg, 0.002 mmol) and $[NBu_4]BAr^F{}_{24}$ (276 mg, 0.25 mmol) was cooled to 0 ºC. A CV was recorded in the absence of acid, in order to obtain a value for i_p. The solution was then treated with aliquots of a 1 M solution of HCl_2CCO_2D in CH_2Cl_2 via a micropipette. After each addition, a CV was collected at ν= 0.5 V/s, and the value of i_c was recorded. Addition of acid continued until the value of i_c/i_p remained constant (See Figure S37).

Scan Rate Dependence for catalysis by $[t\text{-}HFe_2(adt^{NH2})(CO)_2(dppv_2)]^{2+}$, $[t\text{-}H1^{NH2}]^{2+}$. A 2.5-mL CH_2Cl_2 solution of 0.6 mM **1** (1.5 mg, 0.0015 mmol), 0.1 M $[Bu_4N]PF_6$, and a ferrocene reference was cooled to 0 °C and treated with 125 μL of CF_3CO_2H (1200 equiv). Cyclic voltammograms were obtained at a range of scan rates (See Figures S38).

Proton Reduction Catalysis by $[t\text{-}HFe_2(adt^{NH2})(CO)_2(dppv)_2]^{2+}$, $[t\text{-}H1^{NH2}]^{2+}$. A 2-mL CH_2Cl_2 solution of **1** (2.0 mg, 0.002 mmol) and $[NBu_4]BAr^F{}_4$ (414 mg, 0.37 mmol) was cooled to 0 ºC. A CV was recorded in the absence of acid, in order to obtain a value for i_p. The solution was then treated with aliquots of a 5 M solution of CF_3CO_2H in

CH_2Cl_2 via a micropipette. After each addition, a CV was collected at ν = 0.25 V/s, and the value of i_c was recorded. Addition of acid continued until the value of i_c/i_p remained constant.

Proton Reduction Catalysis by [*t*-DFe$_2$(adtND)(CO)$_2$(dppv)$_2$]$^{2+}$, [*t*-D1ND]$^{2+}$. A 3-mL CH_2Cl_2 solution of **1**^{NH} (2.0 mg, 0.002 mmol) and [NBu_4]BAr^F_4 (166 mg, 0.15 mmol) was cooled to 0 ºC. A CV was recorded in the absence of acid, in order to obtain a value for i_p. The solution was then treated with aliquots of a 1.8 M solution of CF_3CO_2D in CH_2Cl_2 via a micropipette. After each addition, a CV was collected at ν = 0.25 V/s, and the value of i_c was recorded. Addition of acid continued until the value of i_c/i_p remained constant. (See Figure S39).

Proton Reduction Catalysis by [Fe$_2$(adt^{NH})(μ-H)(CO)$_2$(dppv)$_2$]BAr$^F_4$, [μ-H1^{NH}]BAr$^F_{24}$. A 5-mL CH_2Cl_2 solution of [μ-H**1**^{NH}]BAr^F_{24} (9.7 mg, 0.005 mmol) and [NBu_4]PF_6 (193 mg, 0.5 mmol) was cooled to 0 ºC. A CV was collected in the absence of acid, in order to obtain a value for i_p. The solution was then treated with aliquots of a 0.25 M solution of HCl_2CCO_2H in CH_2Cl_2 via a micropipette. After each addition, a CV was collected at ν = 0.1 V/s, and the value of i_c was recorded. Addition of acid continued until the value of i_c/i_p remained constant (See Figure S40).

Proton Reduction Catalysis by [*t*-HFe$_2$(pdt)(CO)$_2$(dppv)$_2$]$^+$, [*t*-H2]$^+$. A 4-mL CH_2Cl_2 solution of **2** (4.3 mg, 0.004 mmol) and [Bu_4N]PF_6 (308 mg, 0.0.8 mmol) was cooled to 0 ºC. The solution was then treated with aliquots of a 0.2 M solution of $HBF_4{\cdot}Et_2O$ in CH_2Cl_2 via a micropipette. After each addition, a CV was collected at ν= 0.5 V/s, and the value of i_c was recorded. Addition of acid continued until the value of i_c/i_p remained constant. As the concentration of acid increased, a wave at more negative potential appears, but this is attributed to reduction of protons directly at the glassy carbon electrode (See Figure S41).

Proton Reduction Catalysis by [Fe$_2$(pdt)(μ-H)(CO)$_2$(dppv)$_2$]PF$_6$, [μ-H2]PF$_6$. A 5-mL CH_2Cl_2 solution of [μ-H**2**]PF_6 (9.7 mg, 0.005 mmol) and [Bu_4N]PF_6 (193 mg, 0.5 mmol) was cooled to 0 ºC. A CV was collected in the absence of acid, in order to obtain a value for i_p. The solution was then treated with aliquots of a 0.25 M solution of

HCl_2CCO_2H in CH_2Cl_2 via a micropipette. After each addition, a CV was collected at n = 0.1 V/s, and the value of i_c was recorded. Addition of acid continued until the value of i_c/i_p remained constant (See Figure S42).

Controlled-potential electrolysis of [*t*-HFe$_2$(adt^{NH})(CO)$_2$(dppv)$_2$]$^+$, [*t*-H1^{NH}]$^+$. A two compartment electrolysis cell was used, in which the compartments were separated by a medium glass frit. The main compartment contained three necks, which were fitted with a septum, a reticulated vitreous carbon working electrode (1 cm x 1cm x 0.5 cm) connected to Nichrome wire by Ag epoxy), and a $Ag/AgNO_3$ reference electrode (contained in a Vycor fritted glass tube). The second compartment consists of a glass tube that was fitted with a Pt wire counter electrode.

To the main and Pt compartments of the cell, 10 mL and 7 mL, respectively, of a CH_2Cl_2 solution of 0.1 M $[Bu_4N]PF_6$ / 0.01 M $ClCH_2CO_2H$ was added. The solution was cooled to 0 ºC in an ice bath, and 100 mL of CH_4 was injected as an internal standard. The solution was then electrolyzed at -1.8 V vs $Fc^{+/0}$, until the current remained constant (~ 700 s, 0.21 mA). At this point, **1^{NH}** (0.005 mmol) was added to the cell, causing the current to increase to 1.1 mA. The current gradually decreased, and after 6500 s it was within 5% of the background current. Upon addition of 0.1 mmol of $ClCH_2CO_2H$ (0.2 mL of 0.5 M stock solution), the current once again increased to 1.1 mA and gradually decreased.

During the first 6500 s of the experiment, 500 μL of headspace was periodically removed through the septum, using a Hamilton 500 μL gas-tight syringe, and injected on an Agilent 7820A gas chromatograph. The experimental yield of H_2 was calculated based on the areas of the H_2 and CH_4 peaks. The average current efficiency was calculated to be 99 ± 12 %.

Based on initial electrolysis in the absence of catalyst, 0.21 mA of the total current is due to reduction of protons at the carbon working electrode. Therefore, in turnover number calculations, 0.21 mA was subtracted from the total current, in order to calculate the charge passed due to the catalyst, and therefore the total amount of H_2 produced by the catalyst.

Supporting Electrochemical Data

a.

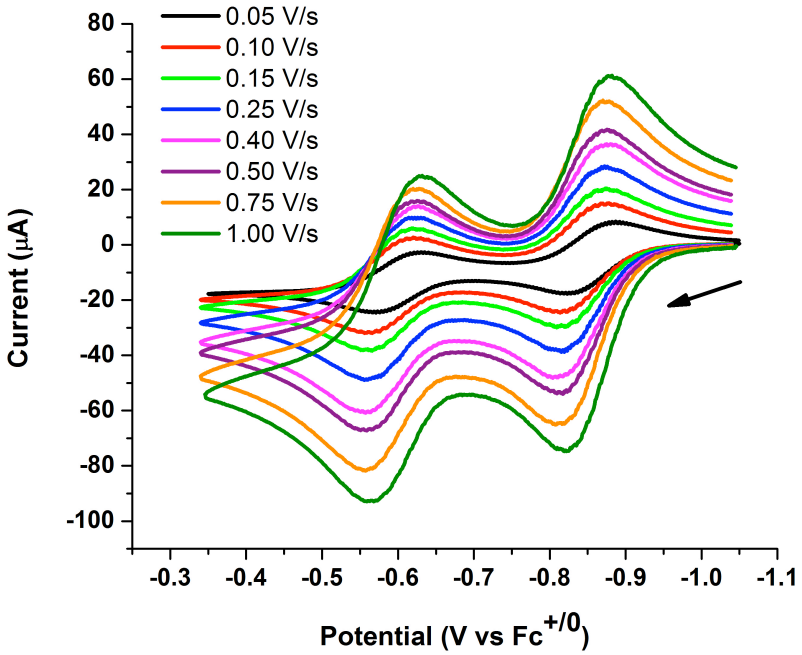

b.

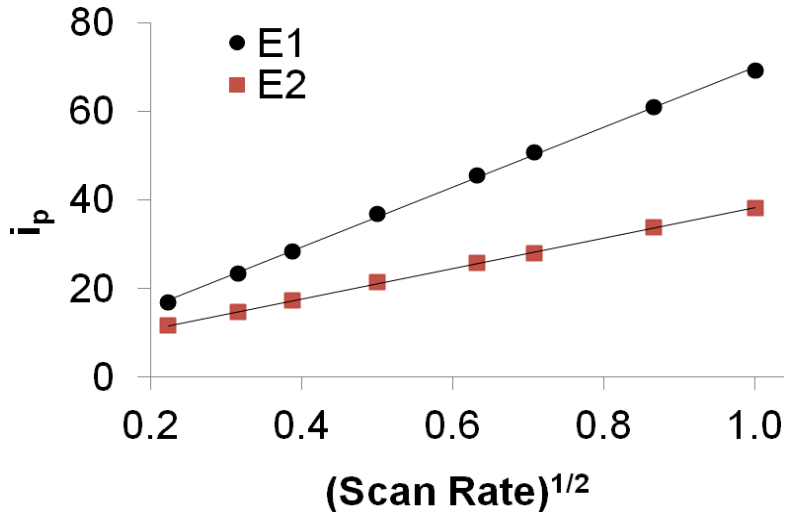

Figure S23. a. Cyclic voltammograms of $\mathbf{1}^{NH}$ at varying scan rates. (Conditions: 0.125 M $[Bu_4N][BArF_{24}]$ in CH_2Cl_2, 1.0 mM $\mathbf{1}^{NH}$, GC working electrode, Pt counter electrode, Ag wire pseudo reference electrode, Fc internal standard) b. Plot of i_p vs. square root of scan rate for $\mathbf{1}^{NH}$.

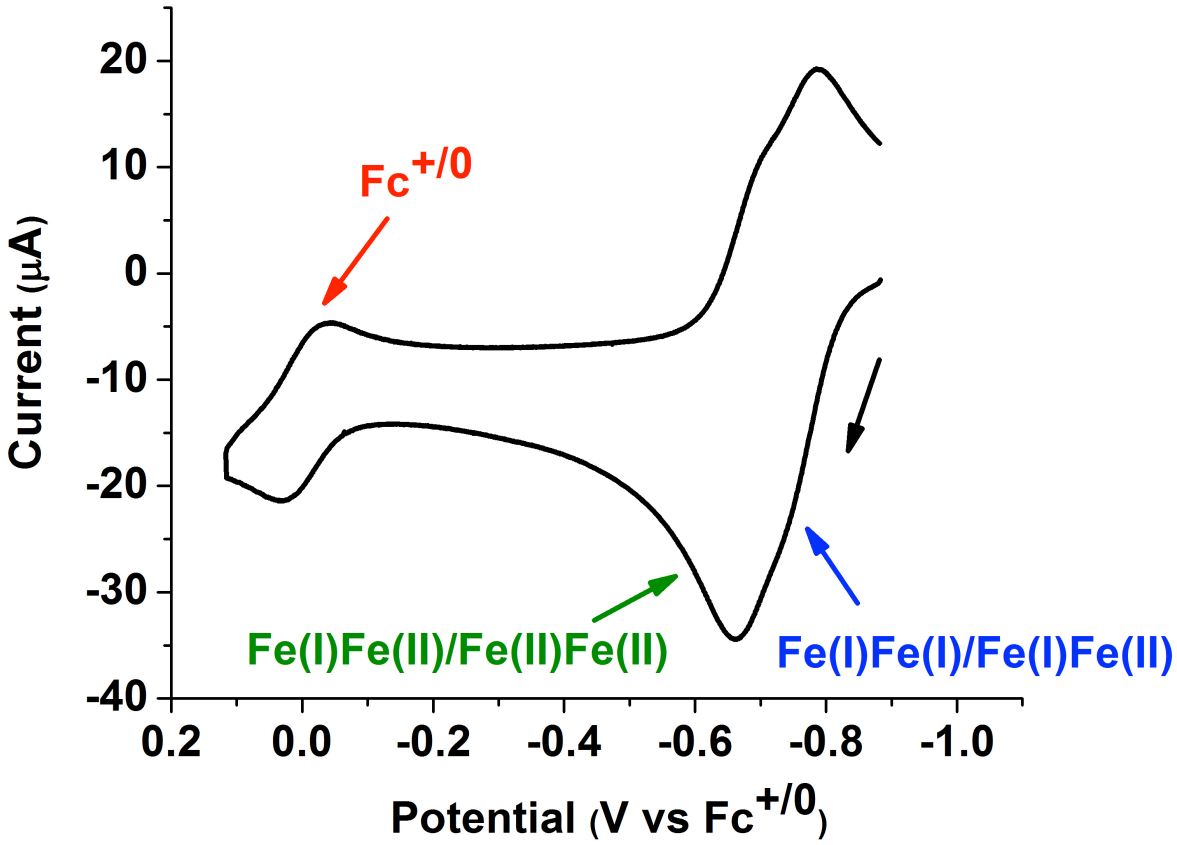

Figure S24. Cyclic voltammogram of $\mathbf{1}^{NH}$, with $[Bu_4N]PF_6$ as supporting electrolyte. (Conditions: 0.1M $[Bu_4N]PF_6$ in CH_2Cl_2, 1.0 mM $\mathbf{1}^{NH}$, GC working electrode, Pt counter electrode, Ag wire pseudo reference electrode, Fc internal standard)

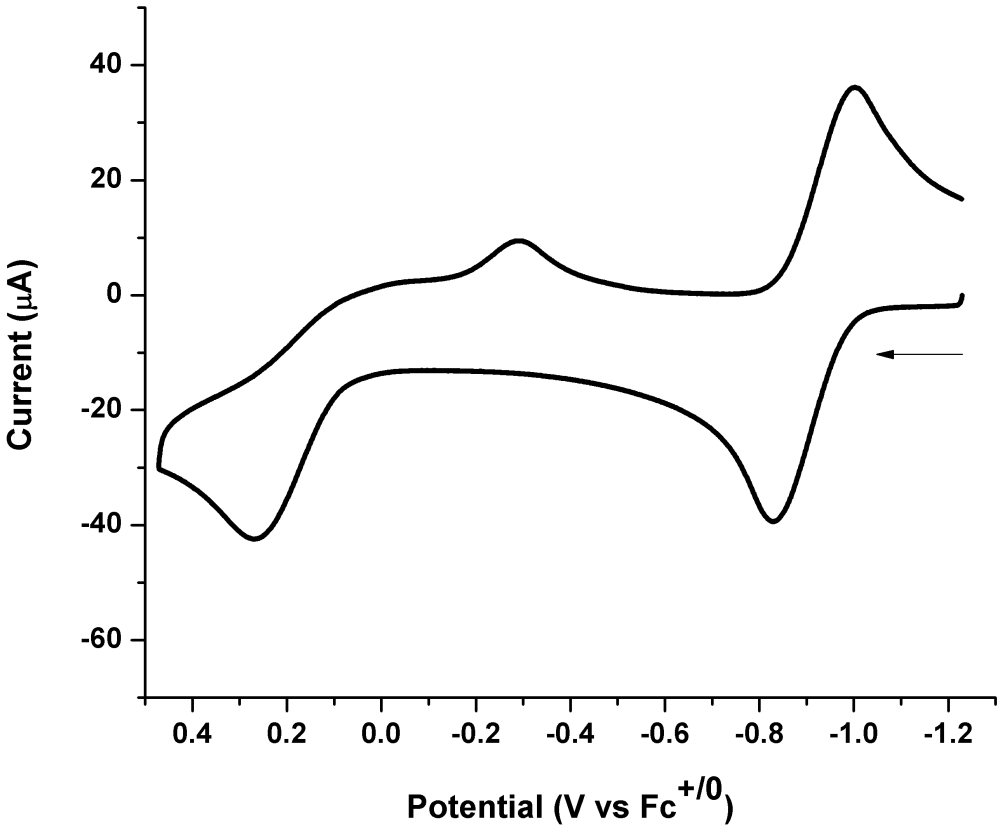

Figure S25. Cyclic voltammograms of **2**. (Conditions: 0.025 M $[Bu_4N][BArF_{24}]$ in CH_2Cl_2, 1.0 mM **1**, GC working electrode, Pt counter electrode, Ag wire pseudo reference electrode, Fc internal standard)

The couples $[\mathbf{1}^{\mathbf{NH}}]^{0/+}$ and $[\mathbf{2}]^{0/+}$ are reversible and occur at highly negative potentials (all potentials are referenced to $Fc^{0/+}$). A quasi-reversible $[\mathbf{2}]^{+/2+}$ couple occurs at a potential ~1 V positive of the first oxidation, whereas $[\mathbf{1}^{\mathbf{NH}}]^{+/2+}$ couple is within 224 mV of the first oxidation. This small $\Delta E_{1/2}$ separating $[\mathbf{1}^{\mathbf{NH}}]^{0/+}$ vs $[\mathbf{1}]^{+/2+}$ might arise from *N*-coordination concomitant with the formation of the dication (Olsen, 2010). With $[Bu_4N]BAr^F{}_{24}$ as the electrolyte, the $[\mathbf{1}^{\mathbf{NH}}]^{0/+}$ and $[\mathbf{1}^{\mathbf{NH}}]^{+/2+}$ couples are reversible and well separated but with $[Bu_4N]PF_6$, the two waves overlap at ~ -0.742 V. The effect of electrolyte on the separation of consecutive redox couples has been described by Geiger et al.(AccChem Res)

Table S1. Electrochemical Properties of **1** and **2**.

Compound	$E_{1/2}$ **in** CH_2Cl_2 **(V vs** $Fc^{+/0}$**)**	**Assignment**	i_{pc}/i_{pa}
$Fe_2(adt)(CO)_2(dppv)_2$, **1**	-0.840, -0.616	$[\mathbf{1}^{NH}]^{0/+}$, $[\mathbf{1}^{NH}]^{+/2+}$	0.78, 0.79
$Fe_2(pdt)(CO)_2(dppv)_2$, **2**	-0.940, 0.124	$[\mathbf{2}]^{0/+}$, $[\mathbf{2}]^{+/2+}$	0.98, irrev

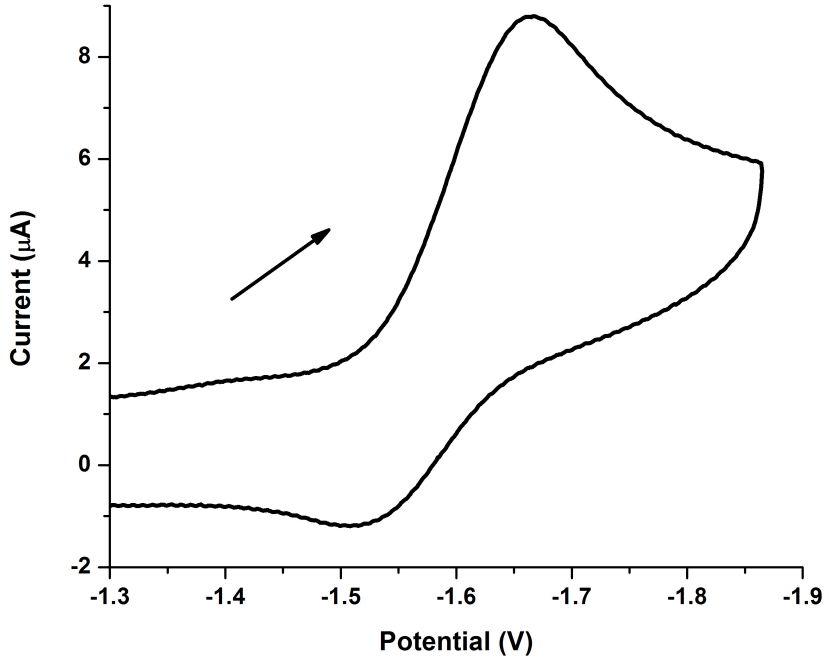

Figure S26. Cyclic voltammogram of [*t*-H**1**^{NH}]$^{+}$ formed *in situ* by addition of 1 equivalent of [H(OEt$_2$)$_2$][BAr^F$_{24}$] to a solution of **1**^{NH} at -78 $^{\circ}$C. (Conditions: 0.036 M [Bu$_4$N][BArF$_{24}$] in CH_2Cl_2, 1.4 mM **1**^{NH}, GC working electrode, Pt counter electrode, Ag wire pseudo reference electrode, Fc internal standard, Scan Rate = 0.5 V/s)

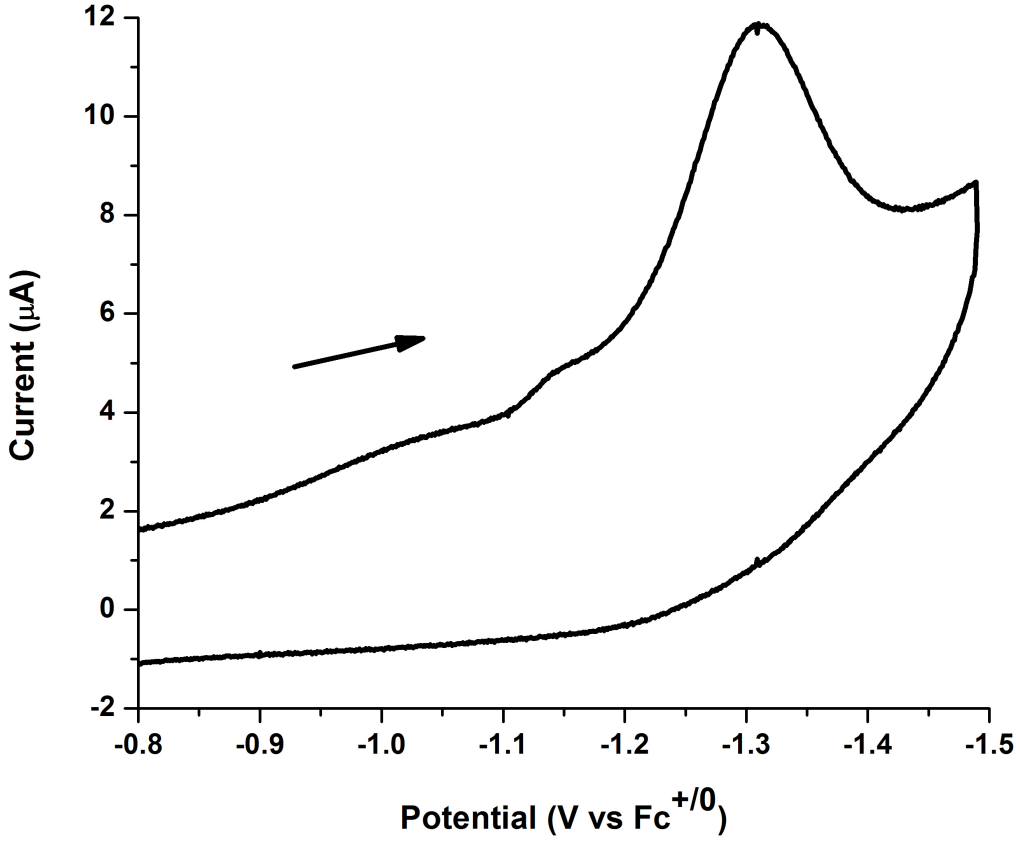

Figure S27. Cyclic voltammogram of [t-H**1**^{NH2}]$^{2+}$ at formed *in situ* by addition of 2 equivalents of $[HOEt_2]BF_4$ to a solution of **1**^{NH} at -78 °C. (Conditions: 0.0125 M $[Bu_4N][BArF_{24}]$ in CH_2Cl_2, 0.5 mM **1**^{NH}, GC working electrode, Pt counter electrode, Ag wire pseudo reference electrode, Fc internal standard, Scan Rate = 0.5 V/s)

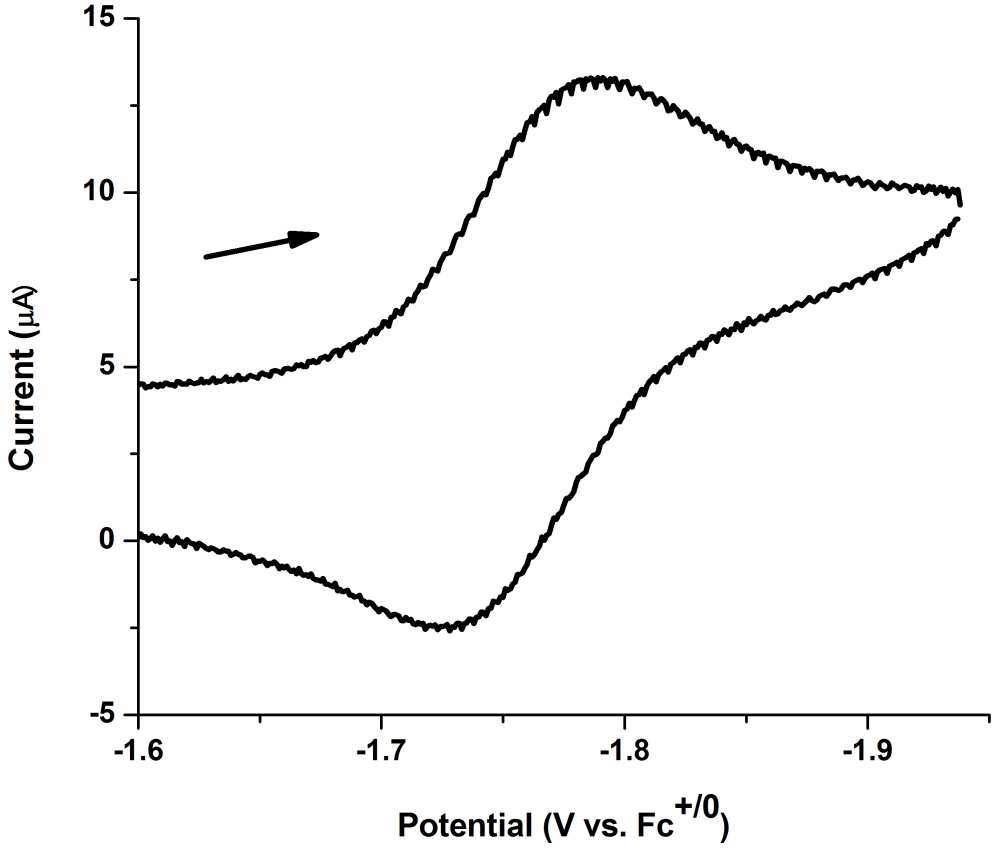

Figure S28. Cyclic voltammogram of [μ-H**1**^{NH}]$^+$ (Conditions: 0.1 M [Bu_4N]PF_6 in CH_2Cl_2, 1.0 mM [μ-H**1**^{NH}]$^+$, GC working electrode, Pt counter electrode, Ag wire pseudo reference electrode, Fc internal standard, Scan Rate = 0.1 V/s)

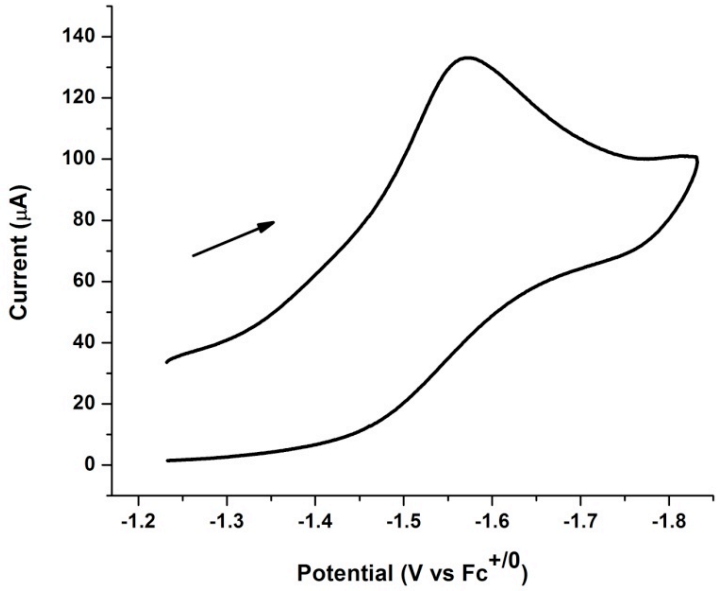

Figure S29. Cyclic voltammogram of [μ-H**1**$^{\mathbf{NH2}}$]$^{2+}$ (Conditions: 0.15 M [Bu_4N][PF_6] in CH_2Cl_2, 2.0 mM [μ-H**1**$^{\mathbf{NH2}}$]$^{2+}$, GC working electrode, Pt counter electrode, Ag wire pseudo reference electrode, Fc internal standard, Scan Rate = 0.5 V/s)

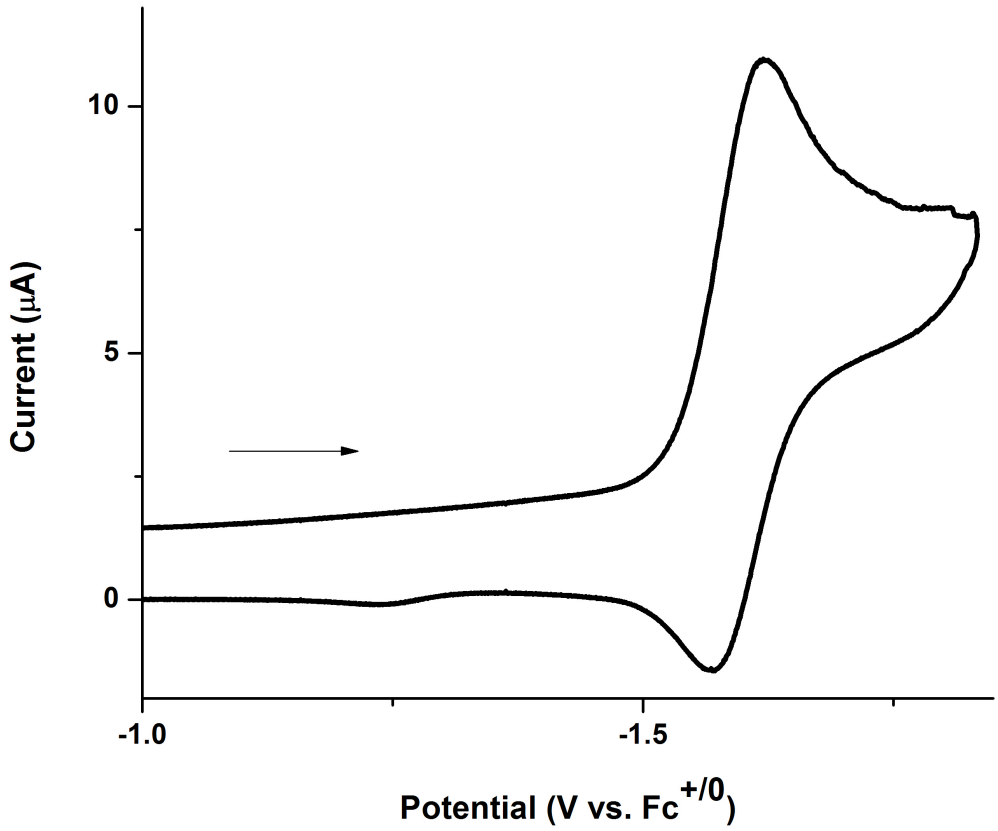

Figure 30. Cyclic voltammogram of [*t*-H**2**]$^+$ formed *in situ* by addition of 1 equivalent of $[H(OEt_2)_2][BF_4]$ to a solution of **2** at -40 °C. (Conditions: 0.1 M $[Bu_4N][PF_6]$ in CH_2Cl_2, 1.0 mM **1**, GC working electrode, Pt counter electrode, Ag wire pseudo reference electrode, Fc internal standard, Scan Rate = 0.1 V/s)

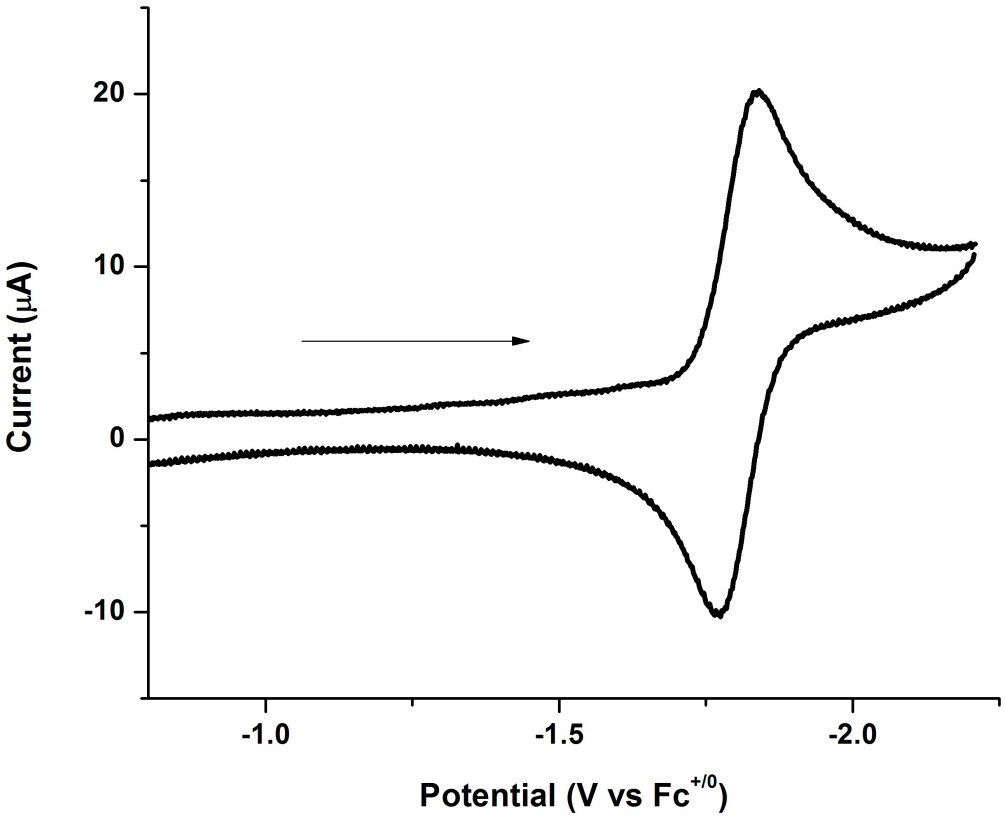

Figure S31. Cyclic voltammogram of [μ-H**2**][PF_6] (Conditions: 0.1 M [Bu_4N][PF_6] in CH_2Cl_2, 1.0 mM [μ-H**2**][PF_6], GC working electrode, Pt counter electrode, Ag wire pseudo reference electrode, Fc internal standard, Scan Rate = 0.1 V/s)

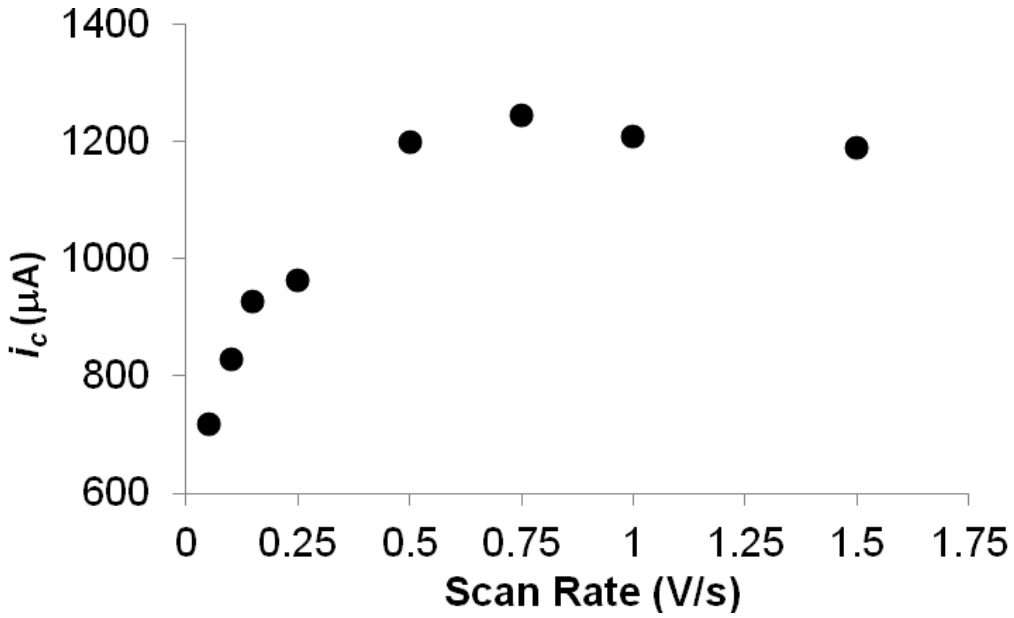

Figure S32. Plot of i_c vs. scan rate for [*t*-H**1**^{NH}]$^+$ (Conditions: 0.125 M [Bu_4N][$BArF_{24}$] in CH_2Cl_2, 1.0 mM **1**^{NH}, GC working electrode, Pt counter electrode, Ag wire pseudo reference electrode, Fc internal standard, 0 °C)

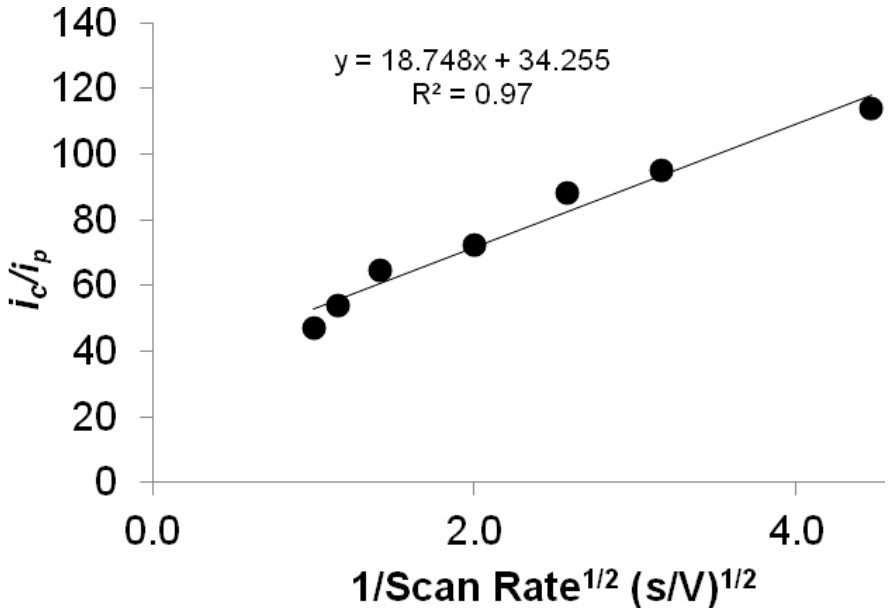

Figure S33. Plot of i_c/i_p vs. 1/scan rate$^{1/2}$ for [*t*-H**1**^{NH}]$^+$ (Conditions see Figure S29).

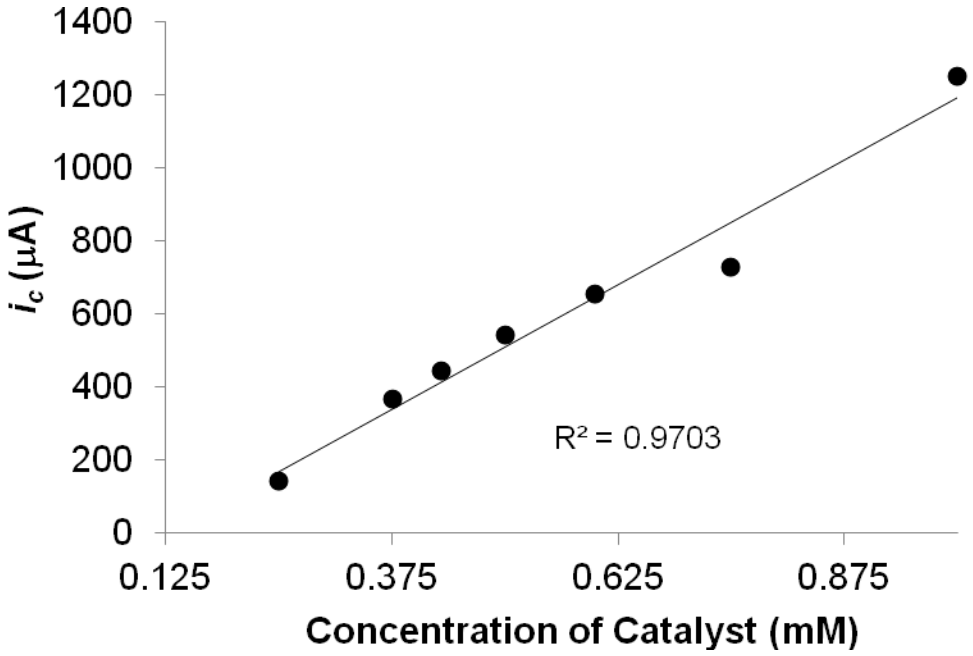

Figure S34. Plot of i_c vs. catalyst concetration for [*t*-H**1**^{NH}]$^+$ (Conditions: 0.125 M [Bu_4N][$BArF_4$] in CH_2Cl_2, 1.0 mmol $H_2ClCCOOH$, GC working electrode, Pt counter electrode, Ag wire pseudo reference electrode, Fc internal standard, 0 °C)

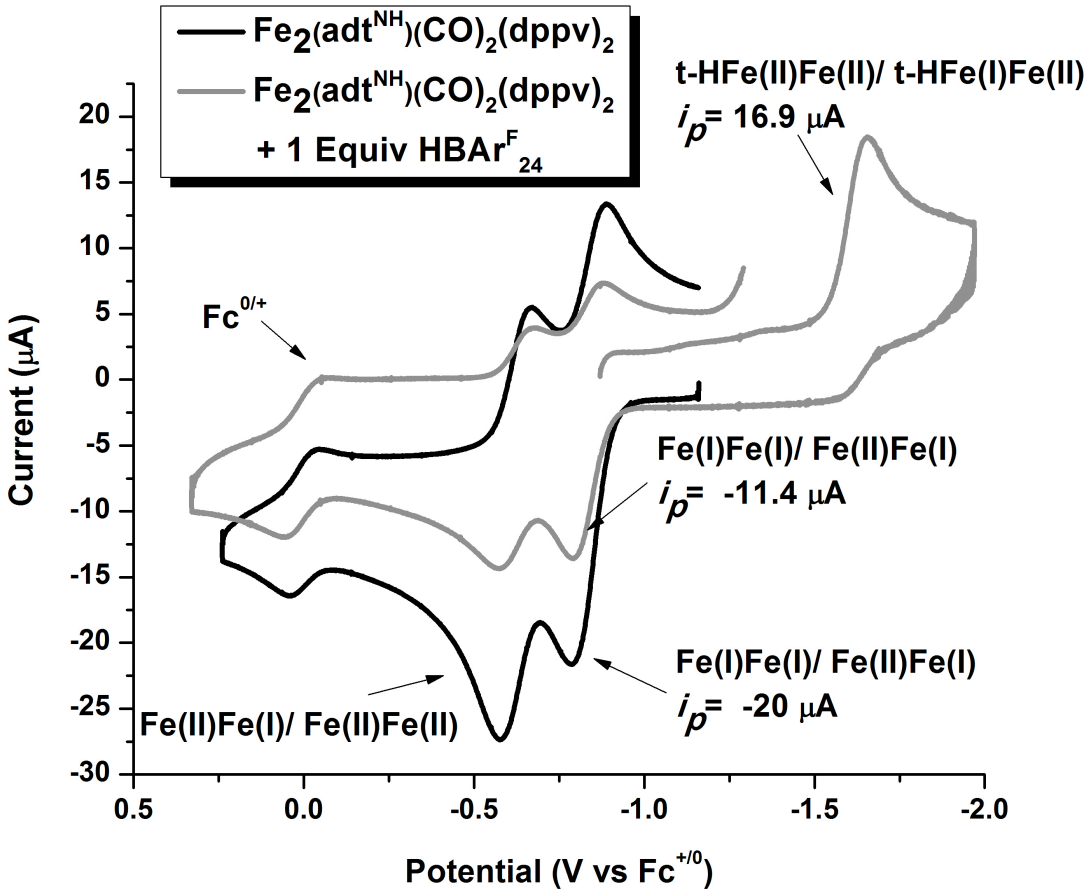

Figure S35. Comparison of *i* for oxidation of **1**^{NH} vs *i* for reduction of [t-H**1**]$^{+}$. We attribute the irreversibility of the *t*-HFe(II)Fe(II)^{NH}/ *t*-HFe(I)Fe(II)^{NH} to a disproportionation reaction, in which H_2 is released, along with ½ an equivalent each of **1**^{NH} and [**1**^{NH}]$^{+}$.

a.

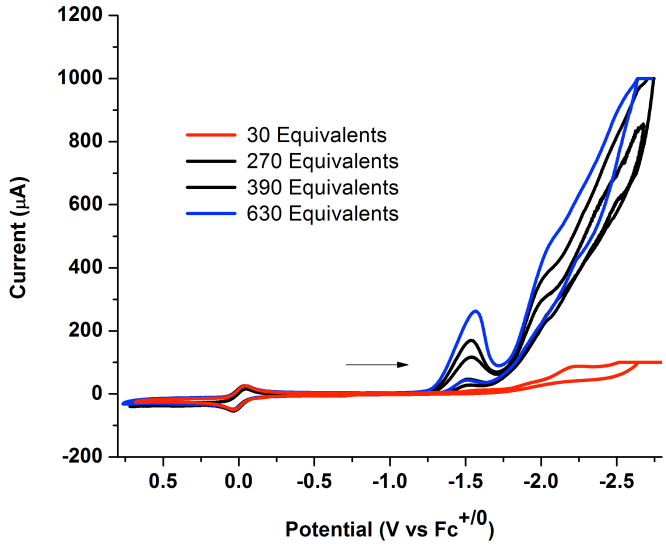

b.

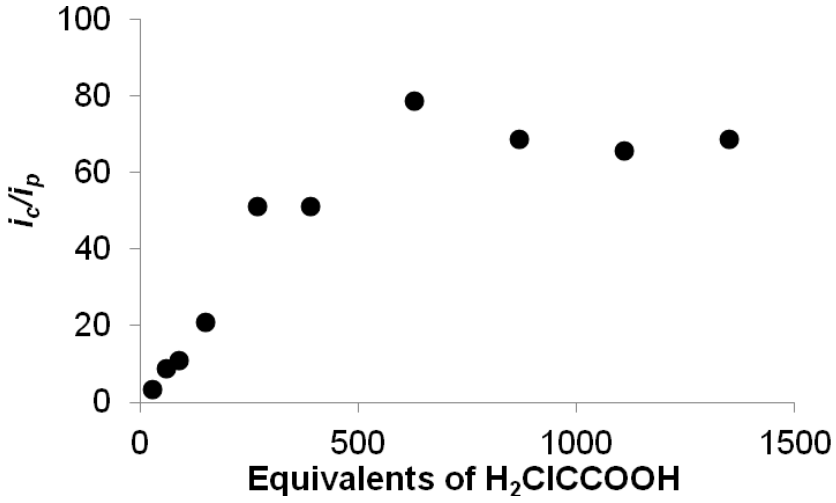

Figure S36. a. Cyclic volatamograms of $Fe_2(adt^{NH})(CO)_2(dppv)_2$ (**1**^{NH}) with increasing amounts of $Cl_2HCCOOH$. (Conditions: 0.1 M $[Bu_4N][PF_6]$ in MeCN, 1.0 mM $[\mu$-**1**H$]^+$, 0 °C, GC working electrode, Pt counter electrode, Ag wire pseudo reference electrode, Fc internal standard, Scan Rate = 0.1 V/s) b. Plot of i_c/i_p vs. equivalents of acid.

a.

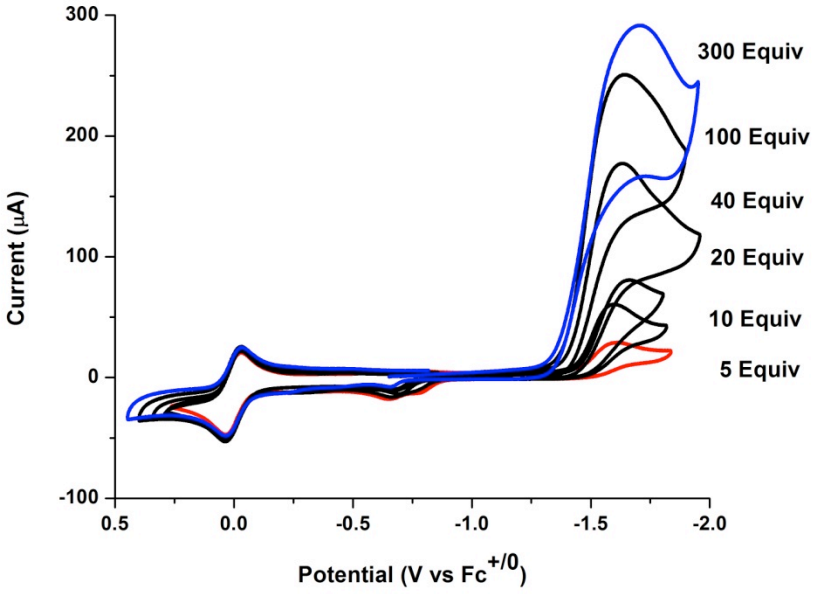

b.

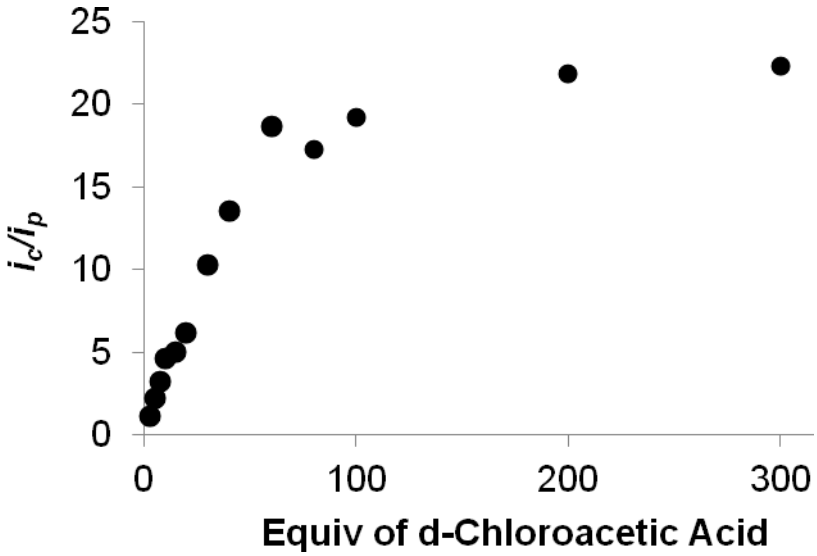

Figure S37. a. Cyclic voltamagrams of a 1.00 mM solution of **1**^{NH} (0 °C, 0.125 M $[Bu_4N][BAr^F{}_{24}]$, CH_2Cl_2, scan rate = 0.5 V/s, GC working electrode, Pt counter electrode, Ag wire pseudo reference electrode, Fc internal standard) recorded with increasing equivs of $ClCH_2CO_2D$. b. Plot of i_c/i_p vs. equivalents of acid.

a.

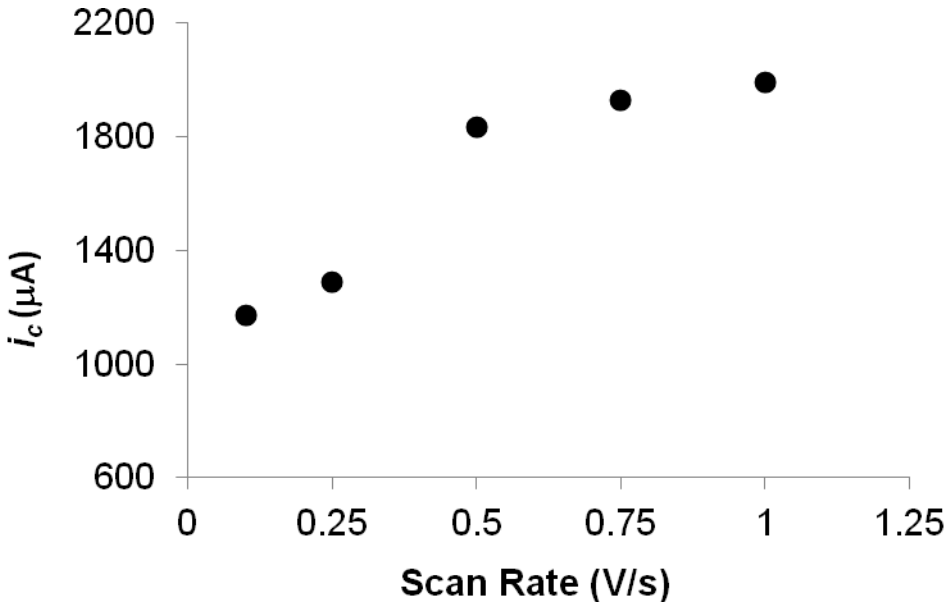

b.

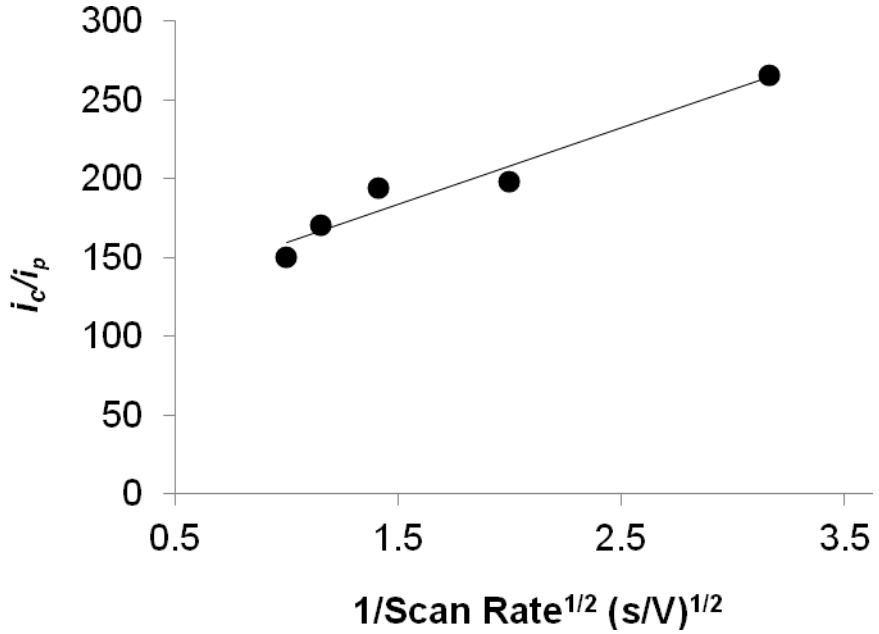

Figure S38. a. Plot of i_c vs. scan rate for [*t*-H**1**$^{\mathbf{NH2}}$]$^{2+}$ (Conditions: 0.1 M [Bu_4N][$BArF_{24}$] in CH_2Cl_2, 0.5 mM **1**$^{\mathbf{NH}}$, GC working electrode, 0.67 M CF_3COOH, Pt counter electrode, Ag wire pseudo reference electrode, Fc internal standard, 0 °C) b. Plot of i_c/i_p vs. 1/scan rate$^{1/2}$ for [*t*-H**1**$^{\mathbf{NH2}}$]$^{2+}$.

a.

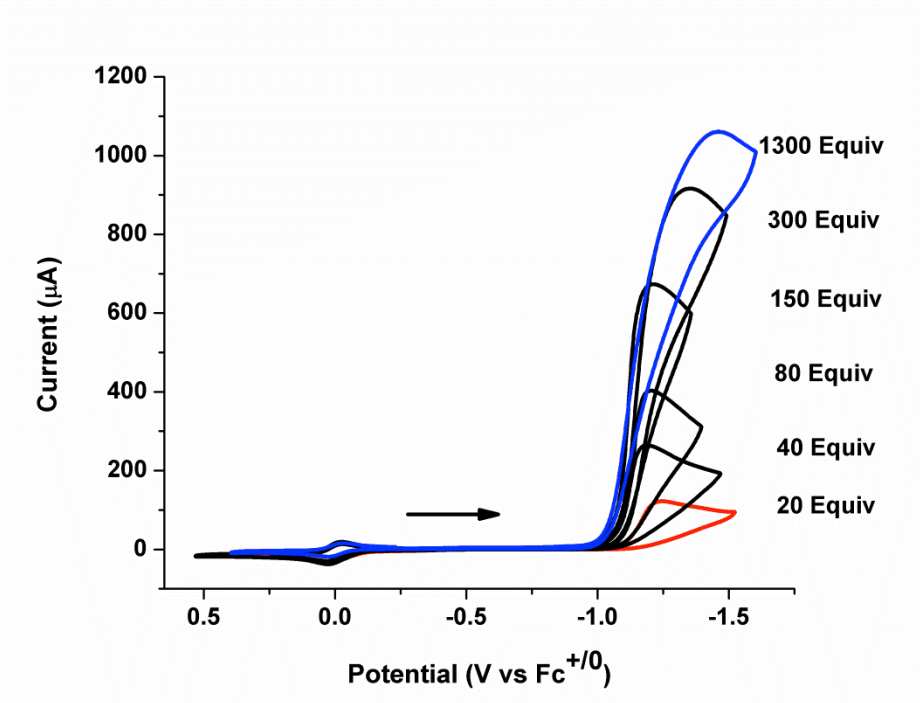

b.

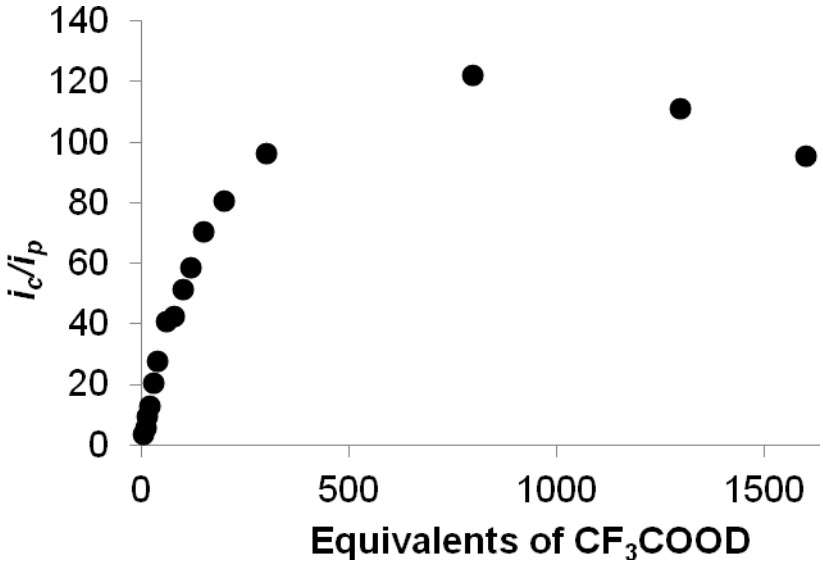

Figure S39. a. Cyclic voltamagrams of a 0.6 mM solution of $\mathbf{1}^{NH}$ (0 °C, 0.005 M $[Bu_4N][BAr^F{}_{24}]$, CH_2Cl_2, scan rate = 0.25 V/s, GC working electrode, Pt counter electrode, Ag wire pseudo reference electrode, Fc internal standard) recorded with increasing equivs of CF_3CO_2D. b. Plot of i_c/i_p vs. equiv of acid.

a.

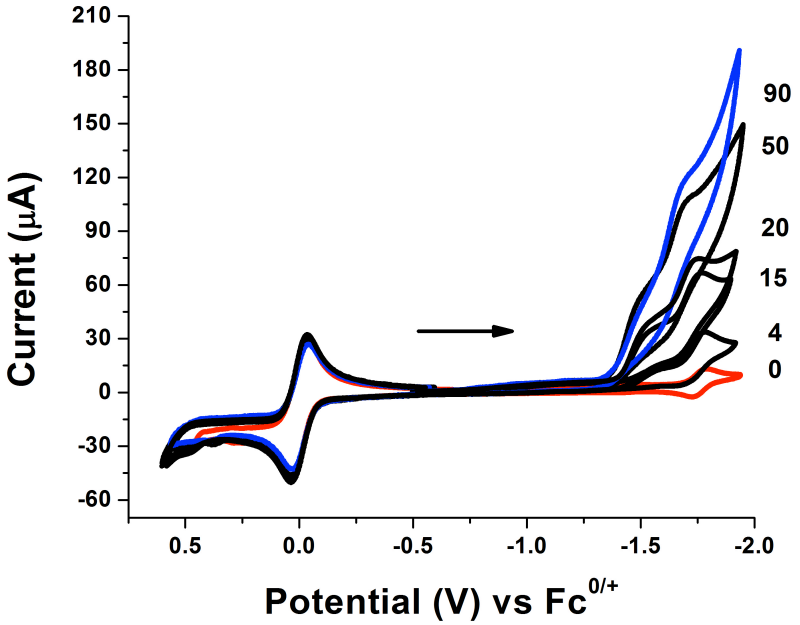

b.

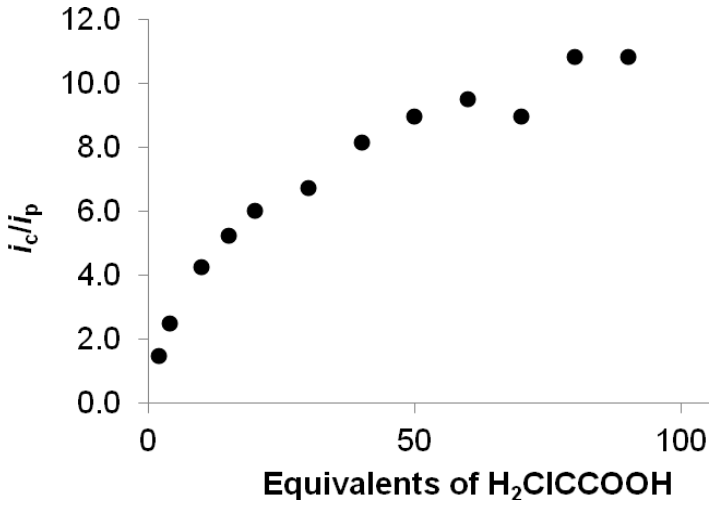

Figure S40. a. Cyclic volatamograms of $[\mu\text{-}HFe_2(adt)(CO)_2(dppv)_2]^+$ ($[\mu\text{-}H\mathbf{1}^{NH}]^+$) with increasing amounts of $Cl_2HCCOOH$. (Conditions: 0.1 M $[Bu_4N][PF_6]$ in CH_2Cl_2, 1.0 mM $[\mu\text{-}\mathbf{1}H]^+$, 0 °C, GC working electrode, Pt counter electrode, Ag wire pseudo reference electrode, Fc internal standard, Scan Rate = 0.1 V/s) (Equivalents of acid indicated to right of each CV) b. Plot of i_c/i_p vs. equivalents of acid.

a.

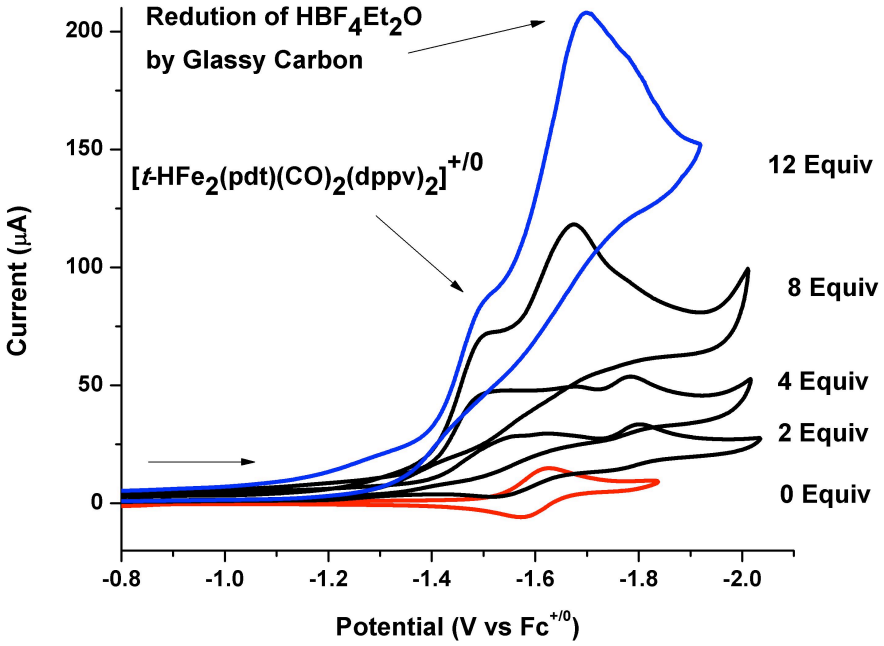

b.

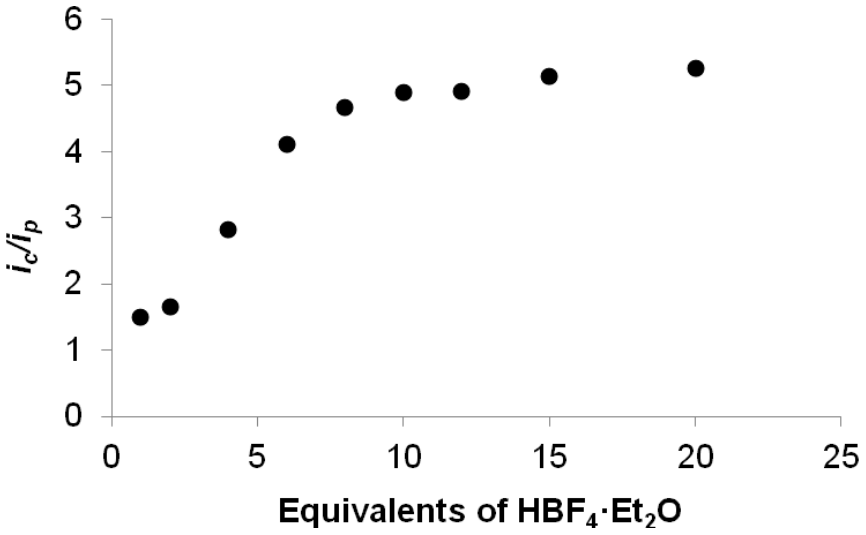

Figure 41. a. Cyclic volatamograms of [*t*-H**2**][BF_4] (generated and *in situ*) with increasing amounts of $HBF_4 \cdot Et_2O$. (Equivalents of acid indicated to right of each CV). (Conditions: 0.1 M [Bu_4N][PF_6] in CH_2Cl_2, 1.0 mM [*t*-H**2**]$^+$, 0 $^\circ$C, GC working electrode, Pt counter electrode, Ag wire pseudo reference electrode, Fc internal standard, Scan Rate = 0.1 V/s) b. Plot of i_c/i_p vs. equivalents of acid.

a.

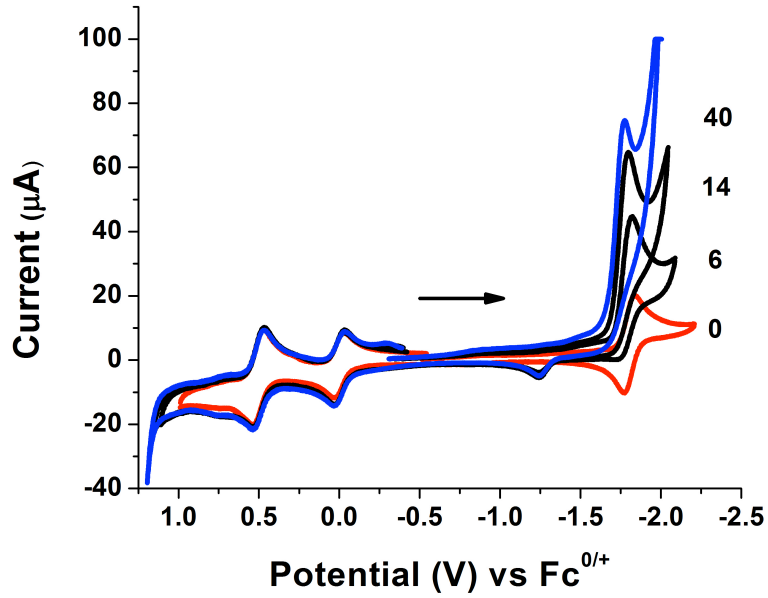

b.

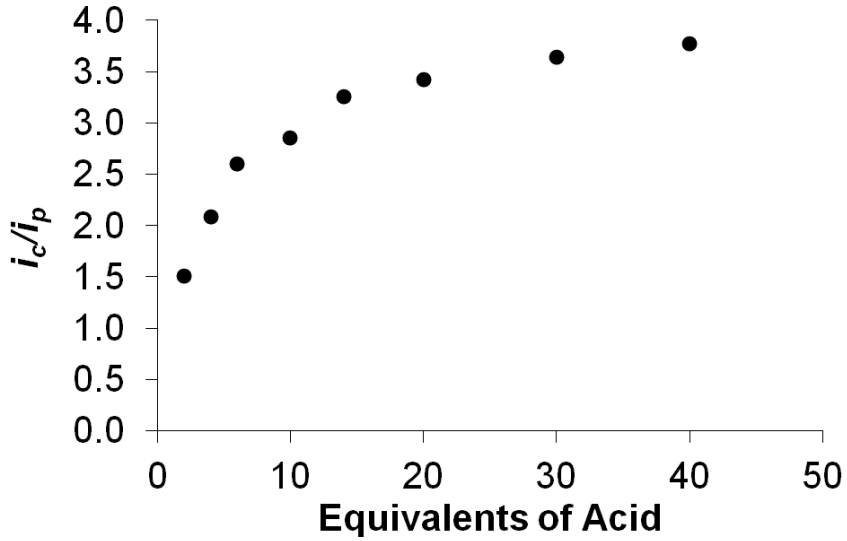

Figure S42. a. Cyclic volatamograms of [μ-H**2**][PF_6] with increasing amounts of $Cl_2HCCOOH$ (Equivalents of acid indicated to right of each CV). (Conditions: 0.1 M [Bu_4N]PF_6 in CH_2Cl_2, 1.0 mM [μ-H**2**]$^+$, 20 °C, GC working electrode, Pt counter electrode, Ag wire pseudo reference electrode, Fc internal standard, Scan Rate = 0.1 V/s) b. Plot of i_c/i_p vs. equivalents of acid.

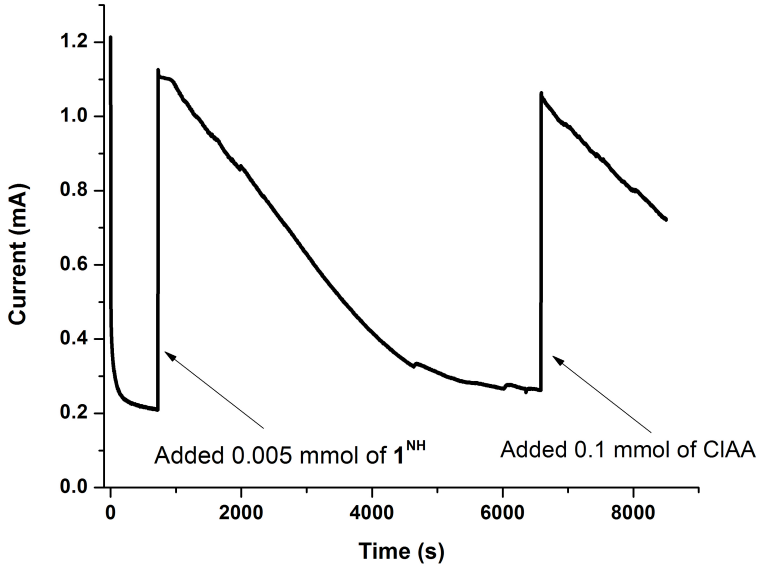

Figure S43. Plot of current vs time for controlled-potential electrolysis of [*t*-H**1**^{NH}]$^{+}$ in a CH_2Cl_2 solution of 0.1 M $[Bu_4N]PF_6$ / 10 mM $ClCH_2CO_2H$.

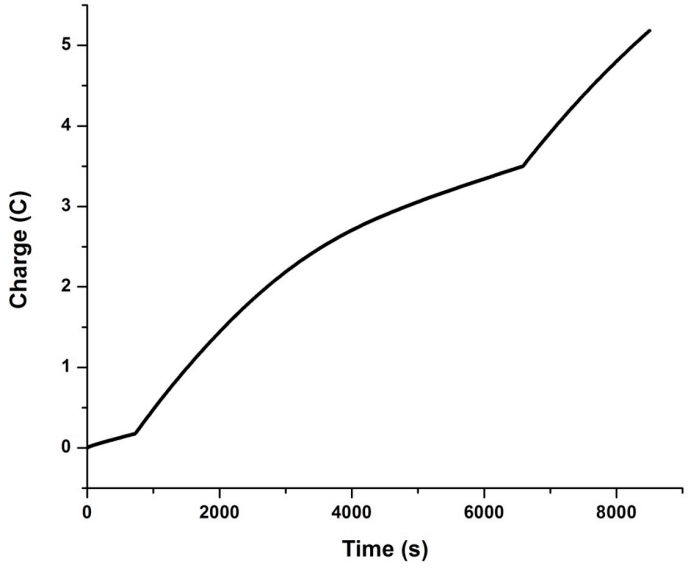

Figure S44. Plot of charge vs time for controlled-potential electrolysis of [*t*-H**1**^{NH}]$^{+}$ in a CH_2Cl_2 solution of 0.1 M $[Bu_4N]PF_6$ / 10 mM $ClCH_2CO_2H$.

Table S2. Experimental results from controlled-potential electrolysis experiment.

Time (s)	1473	4300	5500
Total Charge (C)	0.957	2.823	3.204
Calc mmol H_2	4.96×10^{-3}	1.46×10^{-2}	1.66×10^{-2}
Calc Vol H_2 (μL)	111	328	372
Exp mmol H_2	4.32×10^{-3}	1.48×10^{-2}	1.82×10^{-2}
Exp Vol H_2 (μL)	97	332	408
Efficiency	87	101	110

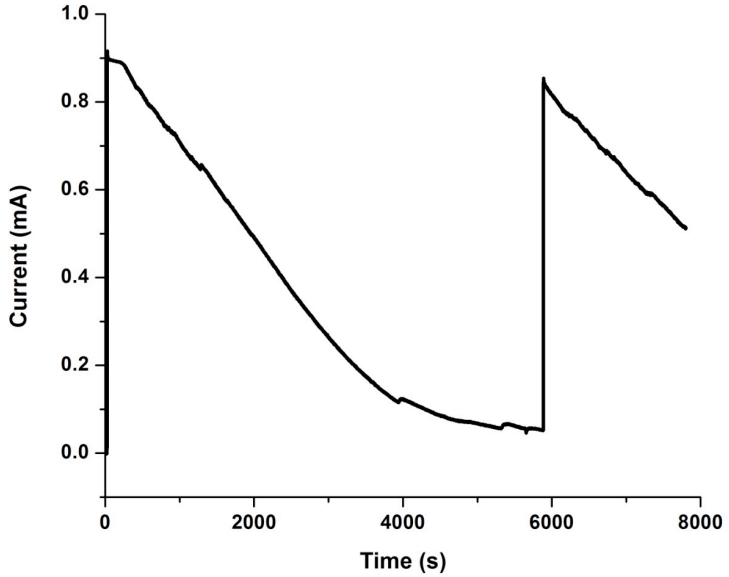

Figure S45. Plot of current vs time for controlled-potential electrolysis of [*t*-H**1**^{NH}]$^{+}$ in a CH_2Cl_2 solution of 0.1 M $[Bu_4N]PF_6$ / 10 mM $ClCH_2CO_2H$. To account for current due to direct reduction of protons at the carbon electrode, 0.21 mA has been subtracted. Time = 0 s corresponds to the time at which catalyst was added to the solution.

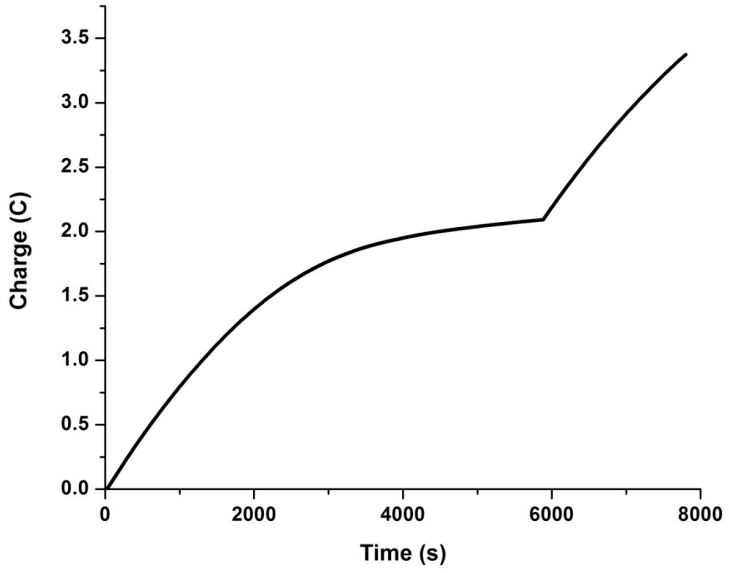

Figure S46. Plot of charge vs time for controlled-potential electrolysis [*t*-H**1**^{NH}]$^{+}$ in a CH_2Cl_2 solution of 0.1 M $[Bu_4N]PF_6$ / 10 mM $ClCH_2CO_2H$, with background correction.

Table S3. Turnover number for catalysis by [*t*-H**1**^{NH}]$^{+}$, based on controlled-potential electrolysis experiment.

Time (s)	773	3600	4800	5800	7800
Charge Due to Catalyst (C)	0.629	1.90	2.02	2.08	3.38
mmol H_2 Due to Catalyst	3.26×10^{-3}	9.85×10^{-3}	1.08×10^{-2}	1.08×10^{-2}	1.75×10^{-2}
Turnover Number	0.65	1.97	2.16	2.16	3.50

References

(1) Li, T.; Lough, A. J.; Morris, R. H. *Chem.Eur. J.* **2007**, *13*, 3796.

(2) Bard, A. J.; Faulkner, L. R. *Electrochemical Methods Fundamentals and Applications*; J. Wiley: New York, 2001.

(3) Pool, D. H.; DuBois, D. L. *Journal of Organometallic Chemistry* **2009**, *694*, 2858.

(4) Felton, G. A. N.; Glass, R. S.; Lichtenberger, D. L.; Evans, D. H. *Inorg. Chem.* **2006**, *45*, 9181.

(5) Fourmond, V.; Jacques, P.-A.; Fontecave, M.; Artero, V. *Inorg. Chem.* **2010**, *49*, 10338.